UNITED NATIONS EDUCATIONAL, SCIENTIFIC AND CULTURAL ORGANIZATION
INTERNATIONAL ATOMIC ENERGY AGENCY
INTERNATIONAL CENTRE FOR THEORETICAL PHYSICS
I.C.T.P., P.O. BOX 586, 34100 TRIESTE, ITALY, CABLE: CENTRATOM TRIESTE

SMR/930 - 40

"Workshop on El Niño, Southern Oscillation and Monsoon"
15 - 26 July 1996

"Intercomparison of the Seasonal Cycle of Tropical Surface Stress Simulated by General Circulation Models"

B.N. GOSWAMI & N.H. SAJI
Centre for Atmopsheric Sciences
IISC
Bangalore, India

Please note: These are preliminary notes intended for internal distribution only.

Intercomparison of the Seasonal Cycle of Tropical Surface Stress Simulated by General Circulation Models

N. H. Saji and B. N. Goswami
Centre for Atmospheric and Oceanic Sciences
Indian Institute of Science
Bangalore
India

Abstract

The mean state of the tropical atmosphere is important as the nature of the coupling between the ocean and the atmosphere depends nonlinearly on the basic state of the coupled system. The simulation of the annual cycle of the tropical surface wind stress by 18 AGCMs is examined and intercompared. The models considered took part in the Atmosphere Model Intercomparison Project (AMIP) and were integrated with observed SST for the decade 1979-1988. Several measures have been devised to intercompare the performance of the 18 models on global tropical as well as regional scales.

In contrast to the older generation low resolution models, most models under consideration simulate stronger than observed annual mean zonal stress averaged over the global tropics. Most models do this consistently over almost all tropical regions except Somali and the equatorial Indian ocean. In these two regions the models tend to underestimate the annual mean zonal stress. The model simulations in these regions are rather unreliable as the intermodel spread is comparable to the common model mean. Although models may have a bias in simulating the area averaged zonal winds, most models tend to simulate the amplitude and spatial pattern of the annual mean zonal winds quite well. For the simulation of the meridional wind stress, it is found that in addition to Somali and equatorial Indian ocean, there exists somewhat higher model to model variations even over South Central Pacific, North-East Pacific and Equatorial Eastern Pacific.

Averaged over the global tropics, the amplitude of the annual cycle of the zonal winds is overestimated by almost all models while that of the meridional winds is overestimated by 11 of the 18 models, the rest underestimating it. While the annual mean is poorly simulated by most models over the Somali and equatorial Indian Ocean, the amplitude of the annual cycle is reasonably well simulated by most models over these regions. For the zonal wind annual cycle amplitude, the inter-model spread is much smaller than the common model mean. For the meridional wind annual cycle too, the intermodel spread is much smaller than the model common mean over almost all regions except the north west Pacific where it is somewhat large.

It is shown that the systematic errors in simulating the surface winds are related to the systematic errors in simulating the ITCZ in it's location and intensity. The diversity in simulation of the surface wind over the Somali and equatorial Indian ocean are related to the diversity of AGCMs in simulating the precipitation zones in these regions.

1 Introduction

Tropical surface winds simulated by Atmospheric General Circulation Models (AGCMs) have attracted greater attention in recent years due to the heightened interest in modeling the coupled ocean-atmosphere system. It is now well established that the unstable coupled modes supported by the tropical ocean-atmosphere system (Hirst, 1986; Hirst and Lau, 1990; Goswami and Selvarajan, 1991; Jin and Neelin, 1993) can cause seemingly insignificant errors in the component models to feedback on each other and amplify leading to the coupled climate state diverging unacceptably from the observed climate, a phenomenon known as 'climate drift'. Therefore tropical surface winds simulated by AGCMs should be thoroughly validated before it is to be used as the atmospheric component in a coupled GCM (CGCM). A useful outcome of validation studies is the information that it provides on the nature of the errors in the simulations, thereby aiding in the further improvement of the model.

A variety of AGCMs have been developed worldwide which differ widely in their spatial resolution and physical parameterization schemes. A systematic intercomparison of these AGCM simulations besides establishing/discounting their fitness to be used in a CGCM has the following outcomes: (1) Since a large number of models with diverse resolution and physical parameterizations are being examined, there is a potential for gaining useful insights into the causes of systematic errors in the simulations, (2) Identification of domains where GCMs in general tend to perform well or poorly. Till date, however, no systematic intercomparison of different AGCM simulations of surface winds have been undertaken. In those studies during the last decade when several AGCMs had been integrated with observed mean global or tropical Pacific sea surface temperature (SST) (Lau,1985; Graham et al, 1989; Latif et al, 1990; Kitoh, 1991; Kleeman et al, 1994), the validation of surface winds were a secondary consideration to the primary motivation of investigating the role of slowly varying boundary conditions (e.g. SST) in forcing the low frequency variability in the tropics (Charney and Shukla, 1981; Shukla, 1981). Goswami et al (1995) examined in detail the simulation of the annual cycle and inter-annual variability of the tropical Pacific surface winds simulated by COLA (Centre for Ocean-Land-Atmosphere Studies) AGCM (this was forced with observed SST from January 1979 to March 1992) with an aim to evaluate it's fitness to be considered

as the atmospheric component of a CGCM. This study reveals some of the common features of the systematic errors found in AGCM simulations of tropical surface winds. They find that the model underestimates the amplitude of the annual cycle in the eastern Pacific Inter Tropical Convergence Zone (ITCZ) region and western Pacific South Pacific Convergence Zone (SPCZ) region. It was also noticed that while the model tends to simulate the pattern of the low frequency variability well, the westerly anomalies associated with the warm phase of the ENSO is generally underestimated. The systematic errors in the simulation of the surface winds were shown to be related to the systematic errors in the model simulated large scale precipitation field.

We investigate here the ability of 18 AGCMs of different complexity in simulating the mean annual cycle of the surface wind stress in the global tropics. The goal is to diagnose the strength and weakness of the GCMs in simulating the present climate so as to determine the best strategy for improving model performance. The models are part of the Atmosphere Model Intercomparison Project (AMIP), under which participating modelling groups carried out a 10-year integration (1979-1988) of AGCMs (Gates, 1992) using daily SST forcing derived from monthly mean observed SST produced by Reynolds (1988). Our work addresses one of the several aspects to be investigated under the AMIP diagnostic subproject entitled "Surface boundary fluxes over the oceans".

The climatological surface winds and their annual cycle demand attention for several reasons. It has been found that the nature of the inter-annual variability simulated by coupled models depends crucially on the strength of the coupling between the component subsystems (Neelin, 1990) which in turn is a non-linear function of the strength of the mean annual cycle. Thus it is not surprising that anomaly models that have the annual cycle prescribed are more successful in simulating the interannual variability. It is also noted that CGCMs that simulate a more realistic annual cycle tend to have better success in simulating the inter-annual variability. It is now well established that coupled air-sea interactions give rise to interannual variability like the ENSO. It is now being realized that coupled air-sea interactions also do substantially influence the spatial structure of the mean tropical ocean-atmosphere system and it's annual cycle (Mitchell and Wallace, 1992; Xie and Philander, 1994, Djikstra and Neelin, 1994, Nigam and Chao, 1996). For example, the movement of the inter-tropical convergence zone (ITCZ) results in latitudinal displacements in the

trade wind belts which are felt at the equator and are intimately related to the annual cycle of the equatorial cold tongue. The persistence of the ITCZ north of the equator in the eastern Pacific has been interpreted in terms of continental asymmetries of up-welling, stratus cover and convergence zones (Mitchell and Wallace, 1992) and air-sea interactions involving evaporation-wind feedback (Xie and Philander, 1994). The annual westward expansion of the cold tongue in this region has been interpreted in terms of wind and SST-gradient feedback (Nigam and Chao, 1996).

Thus, both the observed annual cycle as well as the observed inter-annual variability in the tropics may be understood in terms of coupled air-sea interactions. Nevertheless, a necessary condition (though probably not sufficient one) for coupled modelling is that the individual components simulate the observed annual cycle if forced by observed corresponding boundary conditions. It is through such continuous improvement of the individual components that significant improvement in several coupled models (Mechoso et al 1995) has taken place as compared to those discussed in an earlier review by Neelin et al (1992). Although the simulated annual cycle is much improved compared to before, these coupled models still have significant systematic errors (Mechoso et al, 1995). Motivated by this background, we address the inter-comparison of the annual cycle of surface winds simulated by a large number of AGCMs forced by observed SST. As the models are diverse in resolution and physical parameterizations, a careful analysis of the systematic errors is expected to provide better understanding of the physical processes responsible for these errors.

2 Models, Verification Data and Methodology

Table 1 lists the models used in this study with a brief description of their major characteristics (see Phillips, 1984 for details). The climatology of tropical surface wind stress was calculated for all the models from the monthly mean data supplied to us for the ten-year AMIP test period 1979-1988. It should be mentioned here that the surface stress calculations depends on the boundary layer formulation of the model which varies widely among models. For diagnostic purposes, monthly mean precipitation from all models were obtained, from which the climatological fields were calculated.

For the purpose of verification, we have used surface wind stress calculated from the COADS surface winds (Slutz, 1990) using the bulk aerodynamic formulation with the air density, $\rho = 1.2$

Table 1:

Modeling group	Abbrev.	Resolution[1]	Convection[2]	PBL (TKE scheme)[3]
Bureau of Meteorology Research Centre	BMR	R31L9	Kuo,Tiedtke	
Canadian Climate Centre	CCC	T32L10	MCA	
Centre National de Recherches Meteorologiques	CNR	T42L30	Bough,Gel	Mellor & Yamada (1982)
Commonwealth Scientific and Industrial Organization	CSI	R21L9	AS,Gel	
Colorado State University	CSU	4°x5° L7	AS, MCA	Suarez et al. (1982), Randall et al. (1985)
Dynamical Extended Range Forecasting	DER	T42L18	MCA,Tiedtke	Mellor & Yamada (1982)
European Centre for Medium-Range Weather Forecasting	ECM	T42L19	Tiedtke	
Goddard Laboratory for Atmospheres	GLA	4°x5° L17	AS	Helfand & Labraga (1988)
Goddard Space Flight Center	GSF	4°x5° L20	AS	Helfand & Labraga (1988)
Japan Meteorological Agency	JMA	T42L21	Kuo, Tiedtke	Mellor & Yamada (1982)
Laboratorie de Meteorologie Dynamique	LMD	3.6°x5.6° L11	MCA,Kuo	
Main Geophysical Observatory	MGO	T30L14	Kuo, MCA	
Max Planck Institute for Meteorology	MPI	T42L19	Tiedtke	Randall (1976)
Meteorological Research Institute	MRI	4°x5° L15	AS,MCA	
National Center for Atmospheric Research	NCA	T42L18	Hack	
State University of New York at Albany	SUN	R15L12	MCA	
University of Illinois, Urbana-Champaign	UIU	4°x5° L7	AS,MCA	
United Kingdom Meteorological Office	UKM	2.5°x3.75° L20	GR	

1- Spherical harmonic truncations: R-rhomboidal, T-triangular, L-levels

2- Based largely on the work of Arakawa and Schubert (1974), Betts and Miller (1993), Bougeault (1985), Del Genio and Yao (1988), Geleyn (1987), Gregory and Rowntree (1990), Hack (1994), Kuo (1974), Manabe and Strickler (1964), Tiedtke (1988)

3- References pertain to the scheme to determine vertical diffusion from turbulence kinetic energy (TKE); PBL (Planetary Boundary Layer) Depth is a prognostic variable only in CSU and MRI; Surface fluxes are stability-dependent in all the models

kg m^{-3} and the drag coefficient, C_D = 0.0015. For comparison of the simulated precipitation climatology with the observed we have used the precipitation climatology of Legates and Wilmot (1990).

Our approach at intercomparison employs a few simple statistical indices that capture essential features of the concerned field. We chose three such indices to describe the concerned field. The first quantity is simply the area-averaged mean of the field over the entire tropics and yields information about the overall bias of the simulated field over observations. The spatial spread is the standard deviation of the spatial field from it's area-averaged value. The spatial correlation measures how good the simulated field captures the spatial pattern of the observed field. In section 3, we apply these three measures to intercompare the annual mean of the simulated zonal and meridional tropical wind stress fields with observations. These measures are representative of the whole tropical belt. To examine the spatial distribution of the systematic biases, the area-averaged mean is calculated over 12 selected tropical regions and compared to observations. In section 4, similar analyses is done to examine the amplitude of the annual cycle. In order to measure how the phase of the annual cycle is simulated, the correlation between simulated monthly mean values and corresponding observations is calculated over the 12 regions. In addition, we also compare the westward expansion of annual cycle of the wind in the Pacific and Atlantic with observations. In section 5, an attempt is made to diagnose why model simulations are highly variable over the equatorial Indian Ocean and the Somali region. The systematic errors in simulating the wind stress in the Pacific are also studied and their relationship with systematic errors in simulating the precipitation zones is discussed in section 6. The results are summarized in section 7.

3 Annual Mean

The annual mean is calculated by taking the time average of the 12 monthly mean climatological values. We evaluate the simulation of this quantity by the 18 AGCMs first for the tropics as a whole and then we examine how model simulations vary from each other over different subregions of the tropical domain. The tropical domain is defined to be the region encompassed between 30°N

and 30°S, 0-360°.

a) Overall Performance in the Tropics

The tropical area-averaged mean of the annual mean zonal and meridional stress is calculated for all models and is plotted in figure 1 as a percentage deviation from the observed, with zonal stress bias along the x-axis and meridional stress bias along the y-axis. The observations show up as strong easterlies (-0.035 N m^{-2}) and very weak southerlies (0.006 Nm^{-2}). Note that the tropical area-averaged southerlies are an order of magnitude smaller than the easterlies. This is due to the near cancellation of moderately strong northerlies and southerlies of the same order of magnitude on either side of the equator. The systematic bias in model simulated zonal and meridional annual mean stress has a wide range of values but most models can be seen to be overestimating the zonal stress and underestimating the meridional stress. The NCA model overestimates easterlies the most (a bias of +50%), while CSU has the weakest easterlies (-30%). The DER model produces the strongest northerlies (+25%), while MGO has the weakest southerlies (-50%).

Figure 1 (right panel) plots the bias in spatial spread of the annual mean zonal and meridional stress fields. It is noted that unlike the area-averaged meridional stress, the observed area-averaged spread in the meridional stress is comparable to that of the zonal stress. Most models have a spatial spread that is close to the observed spread. About 14 out of the 18 models have a bias within 20 % of the observed spread. In contrast only 4 out of 18 models were within 20% of the observed area-weighted mean, tending to imply that models are successful in reproducing spatial anomalies of the right magnitude despite their having systematic biases. Whether or not these spatial anomalies are reproduced at the right location as the observations remain to be evaluated. To do this, we calculate the spatial correlation between the observed and the model fields. The coefficients of the spatial (or pattern) correlation is calculated for all models and is plotted as a bar chart in fig 2 with dark bars measuring the correlation for the zonal component and the grey bars that for the meridional component. Most models show good correlation (> 0.9) with observations. The only model fields that have correlations less that 0.9 are those of CSU (0.81) and LMD (0.86) for the u-component and those of CSU (0.87) and MRI (0.89) for the v-component. The good correlations exhibited by the model anomaly fields with the observations and their relative closeness

to the observed spread indicates that despite the systematic biases models are able to capture well the pattern and magnitude of the distribution of spatial anomalies.

b) Regional Performance

In the previous section we evaluated the simulation of the surface stress fields for the tropics as a whole. It is possible that models might perform differently in the different subdomains of the tropical domain. To gain some idea about regional performances we examine the simulation of the local area-averaged annual mean field of surface stress in 12 selected tropical subdomains (see figure 3). At each subdomain we examine how model simulations compare with observations as well as the extent to which model simulations differ among each other. With 18 models and 12 regions to deal with presentation of results becomes a problem. This is overcome by summarising the important features of the distribution of model means. We associate a mean and a standard deviation with the distribution of the 18 model means (area-averaged annual mean), which for convenience sake is called the common model mean and the intermodel spread respectively. The intermodel spread is a measure of the difference between model simulations and when it is a small quantity the common model mean is interpreted to be representative of a majority of the models.

The upper panel of Figure 4 shows the common model mean (grey bar) and intermodel spread (dark thin bar) of the zonal area-averaged stress along with the observed quantity (outlined bar) in the 12 tropical subdomains. The intermodel spread for the zonal area-averaged stress is seen to be a small fraction (< 0.25) of the common model mean over most regions , except over Somali and the equatorial Indian Ocean. Over most of the Pacific domains barring the South East Pacific and the Equatorial Eastern Pacific , the common model means are larger than the observed, implying that a majority of the models overestimate the zonal stress annual mean. Over the Atlantic, the common model mean is close to the observations. In the Indian Ocean domains, the common model mean is smaller relative to the observations, especially in the Somali and the Equatorial Indian Ocean regions. Since the intermodel scatter is high here, it is difficult to interpret the common model mean as being representative of a majority of the models. In the equatorial Indian Ocean, the inter-model scatter is even larger than the observed mean zonal stress.

A similar plot for the meridional stress annual mean is shown in the lower panel of fig 4.

The intermodel scatter is seen to be generally more for the meridional stress than for the zonal stress with the largest occurring over Somali. Over most regions the common model mean is noted to be smaller relative to the observed mean. Over Somali, the common model mean is about 50% weaker than the observed moderately strong southerlies. The intermodel scatter in this region is an astounding 3 times larger than the common model mean and about 1.5 times larger than the observed mean!. The equatorial Indian ocean is equally bad with inter-model scatter being about 60% of the common model mean. South Central Pacific (80%) and North East Pacific (55%) are the other regions where the relative intermodel scatter is greater than 50%.

In the regions (e.g. Somali, Equatorial Indian Ocean, South Central and North East Pacific) where the intermodel scatter is high, it is difficult to interpret the common model mean as being representative of a majority of the models. Nevertheless it reveals the important fact that in these regions models are in great variance with each other, indicating that the dynamics in these regions is relatively less well understood compared to other domains. In a later section we attempt to explore this difference in more detail and try to understand it's connection with the simulation of precipitation in models.

4 Annual Cycle

The tropical surface stress field exhibits variability in a wide range of space and time scales. Predominant among them in most places are fluctuations on the annual time scale. These annual time scale fluctuations have a spatial distribution, being stronger in some places and weaker in others. A measure of this fluctuation is the root mean square difference of the monthly means from the annual mean. This is calculated for the models and observations at all grid points. It is convenient to call this measure the annual variance, though in the strict sense it is the square root of the variance. We study in this section the simulation of the annual variance in the models.

a) Overall Performance in the Tropics

The tropical area-averaged mean of the zonal and meridional stress annual variance is calculated for all models and plotted in the left panel of fig 5 as a percentage deviation from the observed

with zonal stress bias along the x-axis and meridional stress bias along the y-axis. Most models are seen to systematically overestimate the tropical area-averaged annual variance of zonal stress, but such a conclusion cannot be arrived at for the meridional stress. GLA which differs most as far as the u-component is concerned overestimates it by 45%. In the v-component DER overestimates it by 55% while MRI underestimates it by 35%.

The spatial spread of this field for the different models is shown in the right panel of fig 5. It is noticed that the range of variation among models from the observations is more in the zonal component, with the largest deviation exhibited by GLA which overestimates it by 75%. On the other hand the largest variation in the meridional component is is an overestimation of 20% by DER.

Fig 6 shows the pattern correlation of spatial anomalies of annual variance between models and COADS. Compared to the similar plot for the annual mean field (fig 2), there is on the whole lesser correlation with observations. UKM exhibits the largest correlation with the observations for the zonal stress field while LMD has the least correlation. For the meridional stress part, it is MPI that has the largest and CSU the least correlation. Most models exhibit greater than 80% correlation.

b) Regional Performance

We study in this section the variability of model performance in simulating the annual variance in the 12 tropical subdomains. A local area-averaged mean of the observed and model simulated annual variance are calculated. A common model mean based on all model simulations and the inter-model scatter are then calculated. The upper panel of fig 7 shows the observed mean, common model mean and inter-model scatter for simulation of zonal stress annual variance over the 12 regions. It is seen that the inter-model scatter for the zonal stress field is a small fraction (< 0.25) of the common model mean in all the regions, and therefore the common model mean can be taken to be representative of most models. Thus most models overestimate the amplitude of the annual fluctuations of zonal stress in almost all the subdomains except over Somali and the North Central Pacific. A similar scenario for the meridional stress field is shown on the lower panel. In general, as noted for the annual mean field, here too the inter-model scatter in simulating the

annual cycle of the meridional stress is greater compared to that for the zonal stress fluctuations, with the largest relative inter-model scatter occurring over the North West Pacific (45% of the common model mean). Most models are seen to overestimate these fluctuations in many of the subdomains except over Somali, North Central Pacific, Equatorial Eastern Pacific , South Eastern Pacific and the North Atlantic.

The phase of the time series of the climatological zonal and meridional surface stress is another aspect that is required to be simulated well by models. To evaluate how well models simulate the phase, we calculated the anomalies of monthly means from it's annual mean for each model and the time series of the local area-weighted average of these anomalies at each domain was correlated with the corresponding observed time series. Figure 8 shows the correlation coefficients for model zonal stress anomalies at the 12 tropical subdomains. While most model anomalies exhibit good correlation with the observations in most regions, there are 4 regions where the correlation is weaker and also varies a lot among models. These are the Equatorial Indian Ocean, North Central Pacific, North East Pacific and South East Pacific. It can also be noted that some models have near to zero or negative correlations with observations in these regions. Speculations on this aspect of simulations is deferred to a later section. Figure 9 shows similar correlations for the meridional stress. It is seen that in most regions, the phase of the annual cycle of the meridional stress is well simulated by all models. The north-east Pacific seems to be an exception where the mean correlation is weaker and there is a large scatter among the different models. It is rather interesting to note that, while models differ greatly in simulating the annual mean zonal and meridional stress over the Somali region (fig 4), almost all models simulate the phase of the annual cycle correctly.

4.1 Westward Expansion of Pacific and Atlantic zonal stress anomalies E—A

The annual cycle of the equatorial zonal stress of the Pacific and Atlantic are characterized by a westward propagation of westerly anomalies (departure of monthly mean zonal stress from the annual mean) as shown in fig 10, where the time-longitude section of the zonal stress deviations from annual mean averaged between 5°S-5°N is shown. As discussed in the Introduction, air-sea interactions on the annual time scale is capable of giving rise to this phenomenon (Xie and

Philander, 1994: Nigam and Chao, 1996), and hence it is important to examine how models simulate this feature with prescribed SST. The behaviour of the 18 model simulations can be conveniently grouped into 3 types. In the first, the model simulations exhibit propagation of the westerly anomalies in both the Pacific and the Atlantic as in the observations. Models like BMR, CCC, GSF, JMA, etc. belong to this class. In the second type, the propagation is seen only in the Atlantic but not in the Pacific, like in CSU, ECM, MPI, NCA etc. In the last class propagation characteristics are weak or absent in model simulations over both the Pacific and the Atlantic. CNR, CSI, DER, GLA and SUN show this characteristic.

5 Nature of Simulation in Problem Domains: Indian Ocean

From the analyses of previous sections, we have seen that there were some regions where model simulations showed large differences from observations as well as from each other. These regions are examined in more detail in the following sections with the aim of diagnosing the reasons for such behaviour. The regions chosen for detailed analyses are the Somali region, Equatorial Indian Ocean, North Central and South Central Pacific, North East and South East Pacific.

Somali (50°E-70°E, 10°N-25°N)

The annual time series of area-averaged zonal and meridional monthly mean wind stresses are plotted in fig 11. An important characteristic of such time-series in all the regions studied is the predominance of the annual harmonic over the other subharmonics. To capture the essential features of the annual harmonic, viz., it's phase and amplitude, we subject the time series to a harmonic analysis. The phase and amplitude of the annual harmonic for all model simulations as well as the observations are represented as a dial plot in the middle panel of fig 11. A dark thick arrow is chosen to represent the observed harmonic while thin grey arrows represent different model harmonics. It is however difficult to distinguish between the different models in such a plot.

As can be seen from the time-series and the harmonic plots, most models do simulate the phase of the annual cycle reasonably well for both the zonal and meridional stresses. The main discrepancy is in the simulation of the magnitude of these stresses. There is quite a wide

range of variation among different model simulations with respect to this aspect, with most of the models underestimating both the zonal and meridional stresses. To understand this behaviour it is helpful to briefly review the important factors that affect the surface winds over this region. The surface wind dynamics over the Indian Ocean is more complicated than over the other two tropical oceans due to factors associated with the presence of the vast Asian land-mass and the Himalayan orography. During the summer monsoon, land-ocean contrast in heating sets up large scale pressure-gradients which force the surface winds. However these pressure-gradients are significantly modified by the location and magnitude of the continental and oceanic precipitation. Hence it is plausible that the simulated precipitation field would have a strong influence on the model surface winds. It is therefore instructive to examine the model simulated stress fields in relation to their precipitation fields in a few representative models.

Figure 12 plots the climatological precipitation field and the corresponding surface stress field during July from observations and five model simulations. As the model simulations illustrate, precipitation over the monsoon region remains still a major problem. Each of the model simulations are different in one way or the other from the other ones. The best simulation is by JMA, which simulates the position and magnitude of the precipitation maxima over the continents reasonably well despite the simulated equatorial precipitation being weak. The simulated wind field is quite close to the observed one. Continental precipitation near the west coast is completely absent or very weak in the DER simulation: this is probably the cause of the weaker than observed south westerlies off Somali. On the other hand enhanced precipitation over Burma and north of the equator seems to be responsible for the enhanced winds over these regions. The GSF precipitation is almost close to the observed, with the difference that the continental precipitation maxima are simulated a bit to the west and to the south resulting in these features lying over the sea. The wind stress maxima is also simulated a bit to the south compared to the observations. A narrow band of intense precipitation just south of the equator characterises the simulated precipitation field of LMD. Note also the marked decrease of precipitation over the west coast and over Burma and the associated weak south westerlies. Another narrow intense precipitation band seen around 25°N seems to be drawing the strong south westerlies towards it. In MGO, the precipitation over

the west coast of India and over the Burmese peninsula is weaker than observed. There is a large spurious blob of precipitation at $25^{o}N$, 80°E which draws strong south- westerlies towards it.

The lower panel of figure 12 shows the time-latitude section of the zonally averaged precipitation and the zonal stress climatological fields. The wind stress is averaged between 50°E-70°E and represents that off the Somali region, while the precipitation is averaged between 70°E-100°E as the precipitation over this region is expected to have a significant influence over the Somali winds. To distinguish between the two fields, we plot the precipitation as shaded contours and the stress field as thick unshaded contours. From the observations it can be seen that the precipitation maximum which is south of the equator in the early part of the year, moves to the north reaching 20°N during the summer monsoon season. That the observed stress field has a strong relation with the observed precipitation field can be clearly seen by following the time-evolution of the stress field in relation to the precipitation field. Examination of the model simulations further illustrate this point. The DER and MGO simulations present two extreme cases. In the DER simulation, the precipitation and consequently the zonal stress field are confined near the equator during the summer monsoon. On the other hand, the summer monsoon precipitation maxima in the MGO is simulated farther north of the observed position, and it may be noted that the wind stress maxima is also simulated to the north of the observed location. Models that simulate the continental precipitation reasonably well like JMA and GSF are seen to simulate the wind stress field correctly. The westerly stress maximum in the LMD model situated at 20°N is related to the narrow and intense precipitation band to it's north.

From the above discussion it is clear that the systematic errors in the wind stress field is related to the systematic errors in the simulated precipitation field. Given the variety in the simulation of the precipitation field by the different models, it is not surprising that the simulation of stress field differs so widely among the models.

Equatorial Indian Ocean (60°E-100°E, 5°S-5°N)

The annual cycle of zonal stress and meridional stress along with the corresponding annual harmonics over the equatorial Indian ocean are shown in fig 13. Observations show weak easterlies from January till March and westerlies thereafter. There is a large acceleration of the zonal stress

from April till June and later from August till October. A narrow and intense eastward ocean current, known as the Wyrtki Jet is found over the Equatorial Indian Ocean during these westerly stress accelerations. Model simulations are found to vary widely from each other and from the observed curve. This aspect is also revealed in the annual harmonic dial plot in the middle panel. While the observed peak of the annual harmonic occurs in June, the model simulation of this peak varies from May in some model to October in some other model.

As we have noticed, the equatorial Indian Ocean is a region of very weak winds. Here cross-equatorial flow occurs resulting in westerly stress north of the equator and easterly stress south of the equator, during the northern summer. During the northern winter, this pattern is reversed as the pressure gradient across the equator changes sign. The cross-equatorial flow is the result of large scale pressure gradients between the northern and southern hemispheres due to the contrast in heating of the land in the north and the ocean in the south. This basic pressure distribution is strongly modified in regions of strong precipitation, and near the equator it appears to be strongly sensitive to the spatial pattern and magnitude of precipitation field over the equatorial ocean and over the land mass to the north of it. To illustrate this let us look at figure 14 where we have shown the precipitation fields and the corresponding wind stress field during June of observations and a few models. Precipitation has just set over the west coast of India and over Burma in the observations and south westerlies are seen just north of the equator and south easterlies to the south of the equator. But in the MRI simulation, the winds north of the equator are south easterlies and seem to be forced by the strong precipitation at 10°N sitting over the Arabian sea. The situation is similar in the simulation of CSI. In UIU, continental precipitation is very weak, and there is a strong band of precipitation spanning the entire Indian ocean around 5°N. The strong westerlies west of 80°E seems to be related to this pattern of precipitation. A similar scenario is seen in the SUN and NCA simulations, with the difference that there are strong southerlies at the equator forced by the precipitation band sitting just above the equator and precipitation to the south of the equator being weak. Thus the stress pattern near the equator is strongly influenced by the relative position of various precipitation zones near the equator.

The observed weak wind averaged around the equatorial Indian Ocean is due to cancellation

of westerlies to the north and easterlies to the south. The westerlies to the north and the easterlies to the south are sensitive functions of the position and strength of the continental precipitation (strong during summer) and equatorial precipitation (strong during winter). As discussed above, models differ widely in simulating the continental precipitation during summer months. This leads to unrealistic relative strengths of the north and south precipitation maxima resulting in widely different simulations of the equatorial wind. As the Wyrtki jet is very important for the remote forcing of the Bay of Bengal circulation (Godfrey et al, 1995, Mc Creary et al , 1993), simulation of the annual cycle of the weak equatorial wind with it's correct phase may be important for coupled modeling in this region. Due to complex interactions between ocean-land processes and orographic effects, the simulation of the precipitation distribution over the region has remained a challenging problem (WMO, 1994, Sperber and Palmer, 1994). Until the models become capable of simulating precipitation distribution correctly over this region, the simulation of the equatorial winds will remain to be a problem.

6 Precipitation-Surface Stress Relationship in the Pacific

We investigate here the relationship between the simulated climatological fields of precipitation and wind stress over the Pacific. An inspection of the monthly mean climatological fields of precipitation simulated by the different models reveal that the location and spatial pattern of the precipitation zones in the Pacific Ocean are reasonably well simulated unlike in the Indian Ocean. This improvement in the Pacific precipitation simulation is probably because the land and associated topography north of the Indian Ocean has a significant control on the location and magnitude of the precipitation zones over that Ocean, whereas the tropical Pacific Ocean is by and large free of such complications. The discrepancies between the simulated and observed fields of precipitation over the Pacific are hence subtler than that for the Indian Ocean.

North Central Pacific (180°E-140°W, EQ-25°N)

The time series of zonal and meridional monthly mean stresses for all the models as well as the observations averaged over this region is plotted in figure 15 . The observed easterlies are

found to peak in April and then weakens till September, strengthening again thereafter. Many models however are not quite able to capture these features. For example CSU and UIU which have quite weak easterlies too, as well as SUN increase in strength from Jan till July. Some of the other models peak or wane at the right time, but have reduced amplitudes, while others which have the right amplitude show considerable phase shift, as clearly seen from the annual harmonic dial plot in the middle panel. Thus in general, models have problems in simulating the phase or amplitude or both of the zonal stress annual cycle. This is not true however for the meridional stress annual cycle where one finds most models following the same pattern as the observations, the discrepancies being mainly in the amplitude which too is not as varied as that for the zonal stress.

South Central Pacific (180°E-140°W, 25°S-EQ)

In this domain (see figure 16) observations show the weakest easterlies in April and the strongest in August. Stronger than observed easterlies are simulated by most models, the few exceptions being CSI, CSU, GSF, UIU and LMD. The major discrepancy here is in the simulated phases of the annual cycle, the timing of the maximum of the annual harmonic varies from two months earlier to one month later than observed in different models.

In the observed meridional stress time-series, one finds southerlies over this region from June till October, where after they are replaced by northerlies. A large number of models are seen to underestimate the observed southerlies from July till November, the exceptions being ECM, DER and NCA. Most models however capture the phase of the annual cycle pretty well.

To investigate how the wind stress is related to precipitation in the Central Pacific, we examine in figure 17 time-longitude sections of the precipitation field and stress divergence field in the Central tropical Pacific. The precipitation is plotted as shaded thin contours and the divergence field is overlaid on it with thick contours. The main feature of the observed precipitation in this region is the narrow band of intense precipitation (8 mm/day) at 10°N which is present all through the year. This precipitation band is closest to the equator around March and is at it's northernmost position at 15°N by September. Note also the sharp meridional gradient of precipitation in this band. The equator is a region of low precipitation throughout the year while in the south

central Pacific one could see the eastern flank of the precipitation associated with the SPCZ. The precipitation in this region is lowest during the northern summer. Associated features can be seen in the observed field of surface stress divergence. Thus a strong field of convergence co-located with the precipitation band at 10°N is found present throughout the year. The equator is a region of weak convergence from April till August, thereafter having weak divergence. The convergence field co-located with the precipitation zone in the south central ocean is weakest in the northern summer season. Thus the observed precipitation and surface stress divergence field are seen to be strongly linked to each other. Similar relationship is discernible in the simulated fields of precipitation and surface divergence in the models. For example, the realistic time-latitude patterns of divergence in models like DER, ECM, GLA, JMA, MPI, NCA and UKM are related to the reasonably good reproduction of the observed time-latitude pattern of precipitation. These models reproduce the northerly narrow intense band of precipitation, the equatorial precipitation minima and the weakening of the south central precipitation during the northern summer monsoon. Consequently their stress divergence fields reproduce well the strong convergence field in the north, the stress divergence at the equator and the weakening of the south central divergence field during northern summer season. On the other hand, the simulated precipitation fields of models like CCC, SUN ,MGO and UIU which show a diffused pattern of precipitation in the central pacific. The surface stress divergence field is equally diffused lacking the structure we have seen in the observations and the more successful models. As in the Indian ocean, most of the systematic errors in simulation of the surface wind by the AGCMs in the Central Pacific may be attributed to the systematic errors in simulating the large-scale precipitation by the AGCMs.

North East Pacific (140°W-80°W, EQ-25°N)

The annual time series of monthly mean zonal and meridional stress for observations and the 18 GCMs are shown in figure 18. The simulated easterlies are close to or slightly stronger than observations most of the time, except for CSU, ECM, NCA, SUN and LMD. ECM, NCA, SUN and LMD show strong spurious westerlies between July and September. The phase of the annual cycle of zonal stress is reasonably well captured by most models as the accompanying harmonic dials bring out.

The meridional stress time series shows better simulation of the phase of the annual cycle by most models. The domination of southerlies during the summer in the observations is due to the ITCZ being farthest to the north at this time, and the weakening of the northerlies north of the ITCZ. Most model simulations however show weaker than observed southerlies during this time. In UIU and MGO, the balance is upset by northerlies stronger than southerlies resulting in northerly net meridional stress during this period. On the other hand, NCA shows very strong southerlies between April and December. These results are consistent with the inter-model scatter seen in fig 7 and correlations in fig 8 - 9.

South East Pacific (140°W-80° W, 25°N-EQ)

Figure 19 shows the annual time series of monthly mean zonal and meridional stresses for observations and all models. The annual cycle in this region in the observations is smaller compared to the other Pacific domains we have considered so far. The observations show weakest easterlies in March and the strongest in September. The zonal stress is noticeably weak in CSU, and UIU and strongest in SUN and MGO. There is also wide difference among models in the simulation of the phase of the annual cycle, the harmonic dial plot further substantiating this observation.

The observed meridional stress time series shows weak southerlies in March which becomes strongest in September. This behaviour appears well captured by most models, the differences being mainly in the strength of the northerlies. Thus as seen in the harmonic dial plot, the phase shift for most models is at most by a month with the largest phase shift being shown by CSU where strongest northerlies are found in April and the weakest in December. These observations are also consistent with those shown in figs 7 - 9.

Figure 20 is a plot similar to fig 17 for the eastern Pacific. The observed precipitation field over the eastern Pacific is characterized by a narrow strong band of precipitation around 5°N. Precipitation is almost always found north of the equator, except in April when moderate precipitation is found over 5°S. This is associated with the double ITCZ observed during this month. The precipitation band moves slightly to the north with the approach of northern hemisphere summer and reaches it's northernmost latitude at 10°N in September. The observed stress divergence field exhibits related features. A strong convergence field is found to be co-located with the precipitation

maxima around 5°N. The divergence field also exhibits the latitudinal propagation characteristic exhibited by the precipitation field. Moderate divergence is found at and south of the equator at all times except around April when there is moderate precipitation at 5°S. Thus again we can see that the precipitation field and the surface stress field are closely related. This relationship is exhibited by the model simulated fields too. We find that models like CNR, ECM, MPI, UKM, DER, LMD etc which simulate the observed precipitation field well do well also in the simulation of the divergence field. On the other hand models like CCC, SUN, UIU etc which are characterized by weak and diffuse precipitation reproduce the divergence field also poorly.

In conclusion it can be said that the wind stress field and the precipitation field are intimately linked and hence improvement in the simulation of the precipitation field is essential to the good simulation of the surface stress field.

7 Conclusions and Discussions

The ability of 18 AGCMs that participated in the AMIP project in simulating the mean annual cycle of surface winds in the global tropics is investigated. The 18 models considered here are diverse in their resolution as well as complexity of parameterization of the physical processes. The primary objective of the study has been to identify the strengths and weaknesses of the models with a hope to provide the best strategy for improving model performance. It is recognized that the annual cycle of the surface wind stress plays a crucial role in coupled ocean-atmosphere interactions in the tropics. Therefore for coupled modeling studies it is a necessary condition that an AGCM simulate the observed annual cycle of the surface wind when forced by observed SST. Several measures have been devised to intercompare the results of the 18 models. To investigate whether a model simulates the zonal and meridional winds systematically stronger or weaker than observed over the global tropics, the area-averaged annual mean zonal and meridional stresses are compared with observations. Deviation of the annual mean from the area-averaged annual mean yields the spatial distribution of the annual mean pattern. The simulation of the spatial pattern of the annual mean by different models is intercompared in terms of spatial spread and pattern correlation with observations. Continuing with global measures, the simulation of the amplitude of the annual

cycle is intercompared in terms of an area-averaged amplitude, it's spatial spread compared to observations and pattern correlation with observed pattern of the amplitude. In addition to these global measures we also examine the simulation of the annual mean and the annual cycle at 12 selected regions in the tropics.

Averaged over the global tropics, most models tend to simulate stronger easterly zonal winds. This is rather interesting as older generation low resolution models tended to simulate weaker easterlies in general (Latif et al., 1990; Kitoh, 1991; Goswami et al, 1995). Thus the higher resolution new generation models with relatively better physical parameterizations have changed this picture. In fact models that tend to simulate significantly weaker zonal winds (e.g. CSU and SUN) are low resolution models consistent with earlier studies. Most models also tend to underestimate the area-averaged meridional stress. However, this should not be taken very seriously as area-averaged meridional stress is a small quantity due to cancellation of large quantities of opposite sign (northerlies and southerlies on either side of the equator). Although models vary in simulating the area-averaged annual mean, the pattern of the annual mean zonal as well as meridional winds are simulated quite well with the sole exception of CSU.

When the simulation of the annual mean zonal and meridional stress averaged over 12 smaller regions is examined in detail, it becomes apparent that all the models have serious problems in simulating both the wind components over the Somali and equatorial Indian ocean regions. Over the Somali regions, all the models tend to underestimate both the westerly zonal winds and southerly meridional winds. The most disturbing point is that the intermodel spread (or "reproducibility") is either comparable or larger than the common model mean indicating that model simulations differ widely in this region. Similarly, the simulation of zonal winds over the equatorial Indian ocean is underestimated by most models while the simulation of the meridional winds are overestimated by most models. Again, the inter-model spread is comparable to or larger than the common model mean indicating that the reproducibility is very poor even over this region. As far as the zonal winds are concerned all the other regions including the south Indian ocean are well simulated by most models and are quite reproducible. As far as the meridional winds are concerned there exist somewhat higher model to model variability over the south central Pacific, north-east Pacific and

equatorial eastern Pacific.

Averaged over the global tropics, the amplitude of the annual cycle of the zonal winds is overestimated by almost all models while that of the meridional winds is overestimated by 11 of the 18 models, the rest underestimating it. Examination of the amplitude of the annual cycle over the 12 different regions reveal that while the annual mean is poorly simulated by most models over the Somali and equatorial Indian Ocean, the amplitude of the annual cycle is reasonably well simulated by most models over these regions. For the zonal wind annual cycle amplitude, the inter-model spread is much smaller than the common model mean. For the meridional wind annual cycle too, the inter-model spread is much smaller than the model common mean over almost all regions except the north west Pacific where it is somewhat large.

Over the ocean, surface winds are forced either by deep convection leading to low level convergence (Gill, 1980) or by surface pressure gradients caused by SST gradients (Lindzen and Nigam, 1987). Near the vicinity of large land masses, such as in the Indian ocean, the temperature gradient due to land-ocean contrast may also contribute. To gain some insight into the factors behind the systematic errors in simulating the surface winds by the different models, we investigate the relationship between the precipitation and the surface wind both in observations as well as in the model simulations. It is demonstrated that both the location and intensity of westerly zonal winds over the Somali region is closely related to the precipitation over the Indian continent. The models that simulate the location and intensity of the continental precipitation well, also simulate the Somali winds well. Models that simulate the ITCZ during the NH summer either too close to the equator or too weak in strength also simulate Somali jet too close to the equator or too weak in strength. Even in the central and eastern Pacific it is shown that the surface winds are too closely related to the precipitation. The systematic errors in simulating the surface winds are related to the systematic errors in simulating the ITCZ in its location and intensity. The diversity in simulation of the surface winds over the equatorial Indian ocean are also found to be related to the diversity of simulation of the precipitation zones in this region.

Therefore, in order to further improve the simulation of the surface winds by different models it is imperative that the models improve their simulation of large scale precipitation. Major work

is required to improve the simulation of the surface wind in the equatorial and north Indian ocean. With present skill of simulation of the surface wind in this region by different models when perfect ocean boundary conditions are provided indicates that coupled ocean-atmosphere modeling over the Indian region may face serious climate drift problems. However, unlike over the Pacific large scale unstable air-sea interaction is unlikely to operate in this region. Therefore, a coupled model may be able to tolerate larger systematic errors of individual components over this region. Finally, it may be mentioned here that the model simulations described here were carried out more than five years ago. Many models have been undergoing modifications and improvements since then. As a result, many models may have already overcome some of the systematic errors described in this study.

Acknowledgements

The authors are grateful to Peter Glecker for his enthusiastic help in receiving the quality controlled monthly mean output of the models and Larry Gates for allowing us to take part in the AMIP subproject number 5. We also thank the Department of Science and Technology, Government of India for partial support and the Supercomputer Education Research Centre, Indian Institute of Science for providing the computing facilities.

References

Arakawa A, Schubert WH (1974) Interaction of a cumulus cloud ensemble with the large scale environment, Part I., J. Atmos. Sci. , 31 : 674-701.

Betts AK, Miller MJ (1994) The Betts-Miller Scheme, The Representation of cumulus convection in Numerical Models of the Atmosphere, K.A. Emanuel and D. J. Raymond (eds.) , Amer. Meteor. Soc.: 107-121.

Bougeault P (1985) A simple parameterization of the large- scale effects of cumulus convection. Mon. Wea. Rev , 113 : 2108-2121.

Charney JG , Shukla J (1981) Predictability of monsoon. In Monsoon Dynamics (Eds.) J. Lighthill and R. P. Pearce. Cambridge University Press: pp. 99-109.

Del Genio AD, Yao M-S (1988) Sensitivity of a global climate model to the specification of convective updraft and downdraft mass fluxes. J. Atmos. Sci. , 45 : 2641-2688.

Djikstra HA, Neelin JD (1994) Ocean-Atmosphere Interaction and the Tropical Climatology. Part II: Why the Pacific Cold Tongue is in the East. J. Climate, 8: 1343-1359.

Gates WL (1992) AMIP: The Atmospheric Model Intercomparison Project. Bull. Amer. Met. Soc., 73: 1962-1970.

Geleyn J -F (1987) Use of a modified Richardson number for parameterizing the effect of shallow convection. Short-and Medium-Range Numerical Weather Prediction (Special Vol.) T. Matsuno, Ed., J. Meteor. Soc. Japan:141-149.

Gill AE (1980) Some simple solutions for heat-induced tropical circulations. Quart. J. Roy. Met. Soc. , 106 : 447-462.

Godfrey JS, Alexiou A, Ilahude AG, Legler DM, Luther ME, McCreary Jr JP, Meyers GA, Mizumo K, Rao RR, Shetye SR, Toole JH, Wacongne S (1995) The role of the Indian Ocean in the global climate system. Recommendations regarding the global observing system. Report of the Ocean Observing System Development Panel, Texas A & M University, College Station, TX, USA: 89 pp.

Goswami BN, Krishnamurthy V, Saji NH (1995) Simulation of ENSO related surface winds in the tropical Pacific by an AGCM forced by observed SST, Mon. Wea. Rev., 123: 1677-1694.

Goswami BN and Selvarajan S (1991) Convergence feedback and unstable low frequency oscillations in

a simple coupled ocean-atmosphere model, Geophys. Res. Lett., 18: 991-994.

Graham NE, Barnett TP, Chervin RM, Schlesinger ME, Schlese U (1989) Comparisons of GCM and observed surface wind fields over the tropical Indian and Pacific Oceans. J. Atmos. Sci., 46: 760-788.

Gregory D, Rowntree PRR (1990) A mass flux convection scheme with representation of cloud ensemble characteristics and stability dependent closure. Mon. Wea. Rev. , 118 : 1483-1506.

Hack JJ (1994) Parameterization of moist convection in the NCAR Community Climate Model (CCM2). J. Geophys. Res. , 99 : 5551-5568.

Helfrand HM, Labraga JC (1988) Design of a non-singular level 2.5 second order closure model for prediction of atmospheric turbulence. J. Atmos. Sci. , 45 : 113-132.

Hirst AC (1986) Unstable and damped equatorial modes in simple coupled ocean-atmosphere models, J. Atmos. Sci., 43: 606-630.

Hirst AC, Lau KM. (1990) Intraseasonal and interannual oscillations in a simple coupled ocean-atmosphere model, J. Climate, 3: 713-725.

Jin FF, Neelin JD (1993) Modes of interannual tropical ocean-atmosphere interactions-a unified view. Part I Numerical Results, J. Atmos. Sci., 50: 3477-3503.

Kitoh A (1991) Interannual variations in an atmospheric GCM forced by the 1970-1989 SST, Part I: Response of the tropical atmosphere. J. Meteorol. Soc. Japan, 69: 251-269.

Kleeman R, McAvaney BJ, Balgovind RC (1994) Analysis of interannual heat flux response in an atmospheric general circulation model of the tropical Pacific. J. Geophys. Res., 99D: 5539-5550.

Kuo HL (1974) Further studies of the parameterization of the influence of cumulus convection on large-scale flow. J. Atmos. Sci. , 31 : 1232-1240.

Latif M, Biercamp J, von Storch H, McPhaden MJ, Kirk E (1990) Simulation of ENSO related surface wind anomalies with an Atmospheric GCM forced by observed SST., J. Climate, 3: 509-521.

Lau NC (1985) Modeling the seasonal dependence of atmospheric response to observed El Nino in 1962-76, Mon. Wea. Rev., 113: 1970-1996.

Legates DR, Willmott CJ, (1990) Mean Seasonal and spatial variability in gauge-corrected global precipitation. Int. J. Climatol. , 10 : 111-127.

Lindzen RS, Nigam S. (1987) On the role of sea surface temperature gradients in forcing the low-level winds in the tropics. J. Atmos. Sci. , 45 : 2440-2458.

Manabe S, Strickler RF, (1964) Thermal equilibrium of the atmosphere with a convective adjustment. J. Atmos. Sci. , 21 : 361-385.

McCreary JP, Kundu PK, Molinari RL (1993) A numerical investigation of the dynamics, thermodynamics and mixed layer processes in the Indian Ocean. Progr. Oceanogr. , 31 : 181-244.

Mechoso CR, Robertson AW, Barth N, Davey MK, Delecluse P, Gent PR, Ineson S, Kirtman B, Latif M, Le Treut H, Neelin JD, Philander SGH, Polcher J, Schopf PS, Stockdale T, Suarez MJ, Terray L, Thual O, Tribbia JJ (1995) The seasonal cycle over the Tropical Pacific in coupled ocean-atmosphere General Circulation Models, J. Climate, 123: 2825-2838.

Mitchell TP, Wallace JM (1992) The annual cycle in equatorial convection and sea surface temperature, J. Climate, 5: 1140-1156.

Neelin JD (1990) A hybrid coupled general circulation model in El Nino studies, J. Atmos. Sci., 47: 674-693.

Neelin JD, Latif M, Allbaart MAF, Cane MA, Cubasch U, Gate WL, Gent PR, Ghil M, Gordon C, Lau NC, Mechoso CR, Meehl GA, Oberhuber JM, Philander SG, Schopf PS, Sperber KR, Sterl A, Takioka T, Tribbia J, Zebiak SE, (1992) Tropical air-sea interactions in general circulation models, Climate Dynamics, 7: 73-104.

Nigam S, Yi Chao (1996) On the evolution-dynamics of the tropical ocean-atmosphere annual-cycle variability, (submitted to J. Climate).

Philander SGH (1990) El Nino, La Nina and the Southern Oscillation. Academic Press: 289 pp.

Phillips TJ (1994) A summary documentation of the AMIP models. PCMDI Rep. No. 18 , Program for Climate Model Diagnosis and Intercomparison: 343 pp.

Randall D (1976) The interaction of the planetary boundary layer with large-scale circulations. Ph.D. Dissertation , University of California, Los Angeles: 247 pp.

Randall DA, Abeles JA and Corsetti TG (1985) Seasonal simulations of the planetary boundary layer and boundary-layer stratocumulus clouds with a general circulation model. J. Atmos. Sci. , 42 : 641-676.

Reynolds RW (1988) A real time global sea surface temperature analysis, J. Climate, 1: 75-86.

Shukla J (1981) Dynamical predictability of the monthly means. J. Atmos. Sci., 38: 2547-2572.

Slutz RJ, Lubkar SJ, Hiscox Jd, Woodruff SD, Jenne RL, Joseph DH, Steurer PM, Elms JD (1985) Comprehensive Ocean-Atmosphere Data Set. Release I, NOAA Environmental Research Laboratories . Climate Research Program, Boulder, CO: 268 pp.

Sperber KR, Palmer TN (1994) Atmospheric Model Intercomparison Project: Monsoon simulations. In Proc. Int. Conf. on Monsoon Variability and Prediction . Trieste, May 9-13, WMO/TD-619 : 601-660.

Suarez MJ, Arakawa A, Randall DA (1983) Parameterization of the planetary boundary layer in the UCLA general circulation model: Formulation and results. Mon. Wea. Rev. , 111 : 2224-2243.

Tiedtke M (1988) Parameterization of the planetary boundary layer in large-scale models. Physically -Based Modelling and Simulation of Climate and Climate Change, Part I, M. E. Schlesinger (ed.): 375-432.

WMO (1994) Proc. Int. Conf. on Monsoon Variability and Prediction, Trieste, May 9-13, 1994. WMO/TD-619.

Xie S-P, Philander SGH (1994) A coupled ocean-atmosphere model of relevance to the ITCZ in the eastern Pacific. Tellus, 46A: 340-350.

Figure Legends

Fig.1. Tropical area-averaged mean and standard deviation (spread) of zonal and meridional stress (Nm^{-2}) annual mean fields for the 18 models plotted as a percentage deviation from the observed value.

Fig.2. Correlations between model simulated and observed fields of annual mean spatial anomalies. Dark bars measure the correlation coefficient for the zonal component while grey bars measure that for the meridional component.

Fig.3. The 12 tropical subdomains selected for detailed analysis.

Fig.4. Observed mean (outlined bar), common model mean (grey bar) and intermodel spread (dark line) for the tropical area-averaged annual mean zonal and meridional stresses (Nm^{-2}) at 12 tropical subdomains.

Fig.5. Tropical area-averaged mean and standard deviation (spread) of zonal and meridional stress (Nm^{-2}) annual variance fields for the 18 models plotted as a percentage deviation from the observed value.

Fig.6. Correlations between model simulated and observed fields of annual variance spatial anomalies. Dark bars measure the correlation coefficient for the zonal component while grey bars measure that for the meridional component.

Fig.7. Observed mean (outlined bar), common model mean (grey bar) and intermodel spread (dark line) for the tropical area-averaged zonal and meridional annual variances (Nm^{-2}) at 12 tropical subdomains.

Fig.8. Correlation coefficients between simulated monthly anomalies of zonal wind stress from it's annual mean and observations for the 18 models at the 12 tropical subdomains. Model identification numbers (1 to 18) are same as shown in fig.5

Fig.9. Correlation coefficients between simulated monthly anomalies of meridional wind stress from it's annual mean and observations for the 18 models at the 12 tropical subdomains. Model identification numbers (1 to 18) are same as shown in fig.5

Fig.10. Time-longitude section of zonal stress anomalies (Nm^{-2}) (departure of monthly means from annual mean) averaged between 5°S-5°N in the Pacific and Atlantic basins.

Fig.11. Annual time-series of zonal and meridional monthly mean stresses (Nm^{-2}) averaged over Somali. The corresponding annual harmonics are plotted in the middle, with the thick arrow representing that of the observations and the thin arrows representing that of the different models.

Fig.12. Monthly mean precipitation (shaded contours, mm/day) and vectors of surface stress (Nm^{-2}) from observations and from 5 selected model simulations for July. The time-latitude section of precipitation (shaded contours) versus zonal stress (in thick contours) is shown in the bottom panel.

Fig.13. Same as fig.11 but for the equatorial Indian ocean.

Fig.14. Monthly mean precipitation (shaded contours, mm/day) and vectors of surface stress (Nm^{-2}) from observations and from 5 selected model simulations for June.

Fig.15. Same as in fig.11 but for the North Central Pacific.

Fig.16. Same as in fig.11 but for the South Central Pacific.

Fig.17. Time-latitude section of longitudinally-averaged (over 180°-140°W) precipitation (shaded thin contours, mm/day) and stress divergence (Nm^{-3}) multiplied by 10^7 (thick contours) in the Central Pacific.

Fig.18. Same as in fig.11 but for the North East Pacific.

Fig.19. Same as in fig.11 but for the South East Pacific.

Fig.20. Time-latitude section of longitudinally-averaged (over 140°W-80°W) precipitation (shaded thin contours, mm/day) and stress divergence(Nm^{-3}) multiplied by 10°7 (thick contours) in the Eastern Pacific.

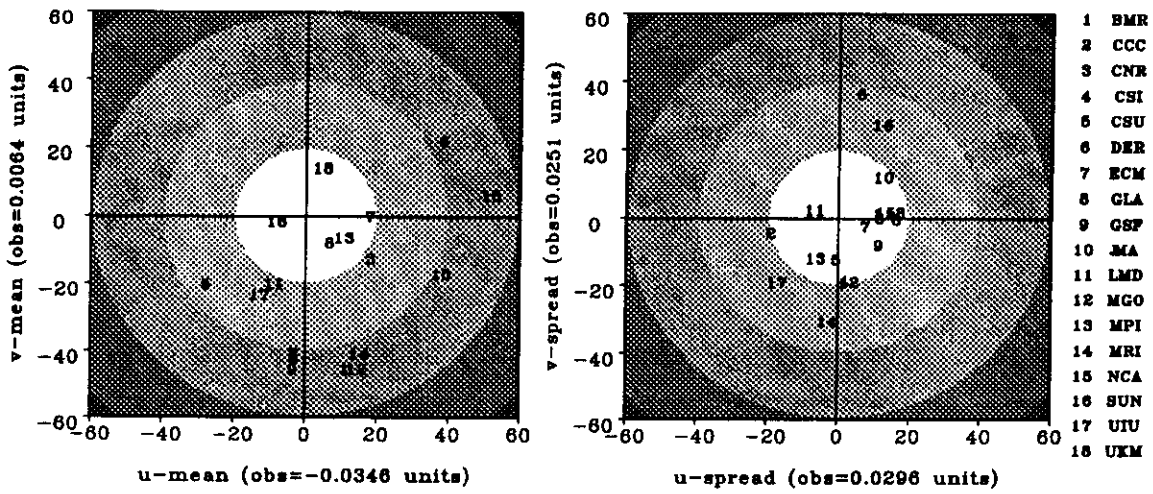

Figure 1: Tropical area-averaged mean and standard deviation (spread) of zonal and meridional stress (Nm^{-2}) annual mean fields for the 18 models plotted as a percentage deviation from the observed value.

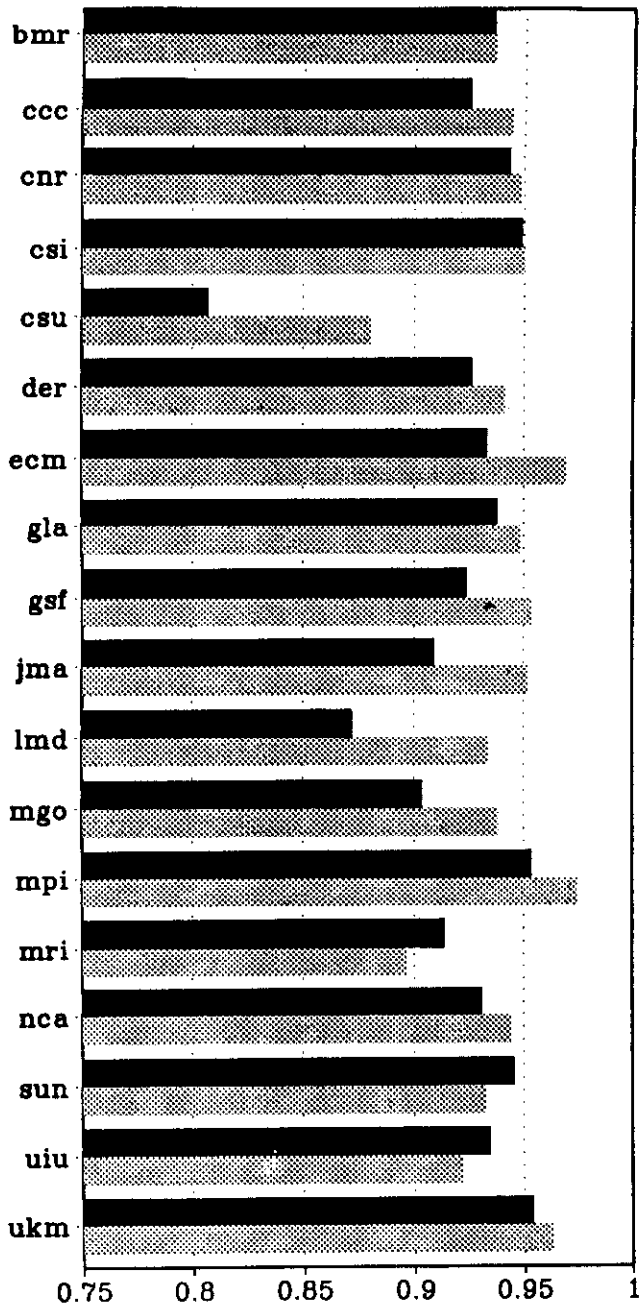

Figure 2: Correlations between model simulated and observed fields of annual mean spatial anomalies. Dark bars measure the correlation coefficient for the zonal component while grey bars measure that for the meridional component.

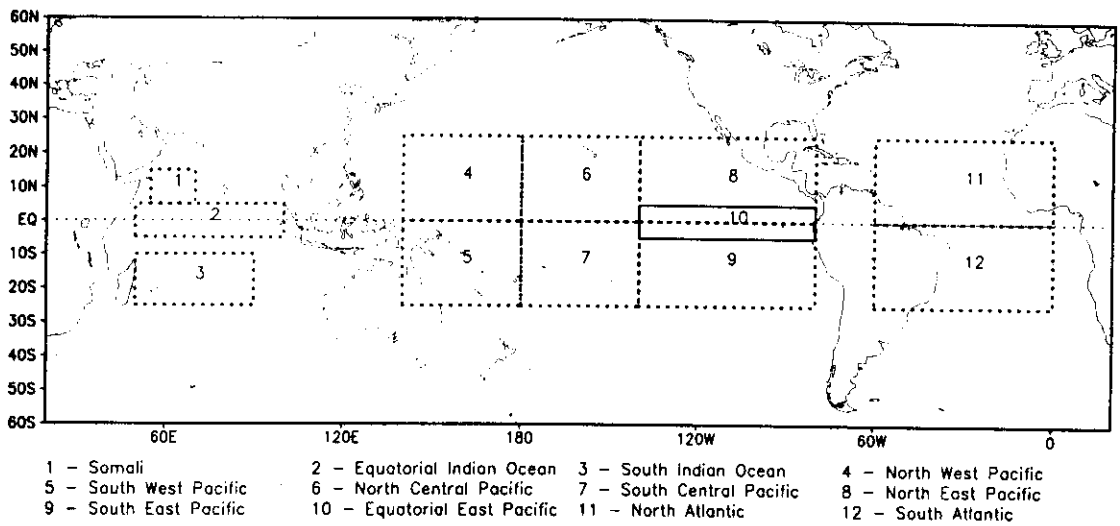

Figure 3: The 12 tropical subdomains selected for detailed analysis.

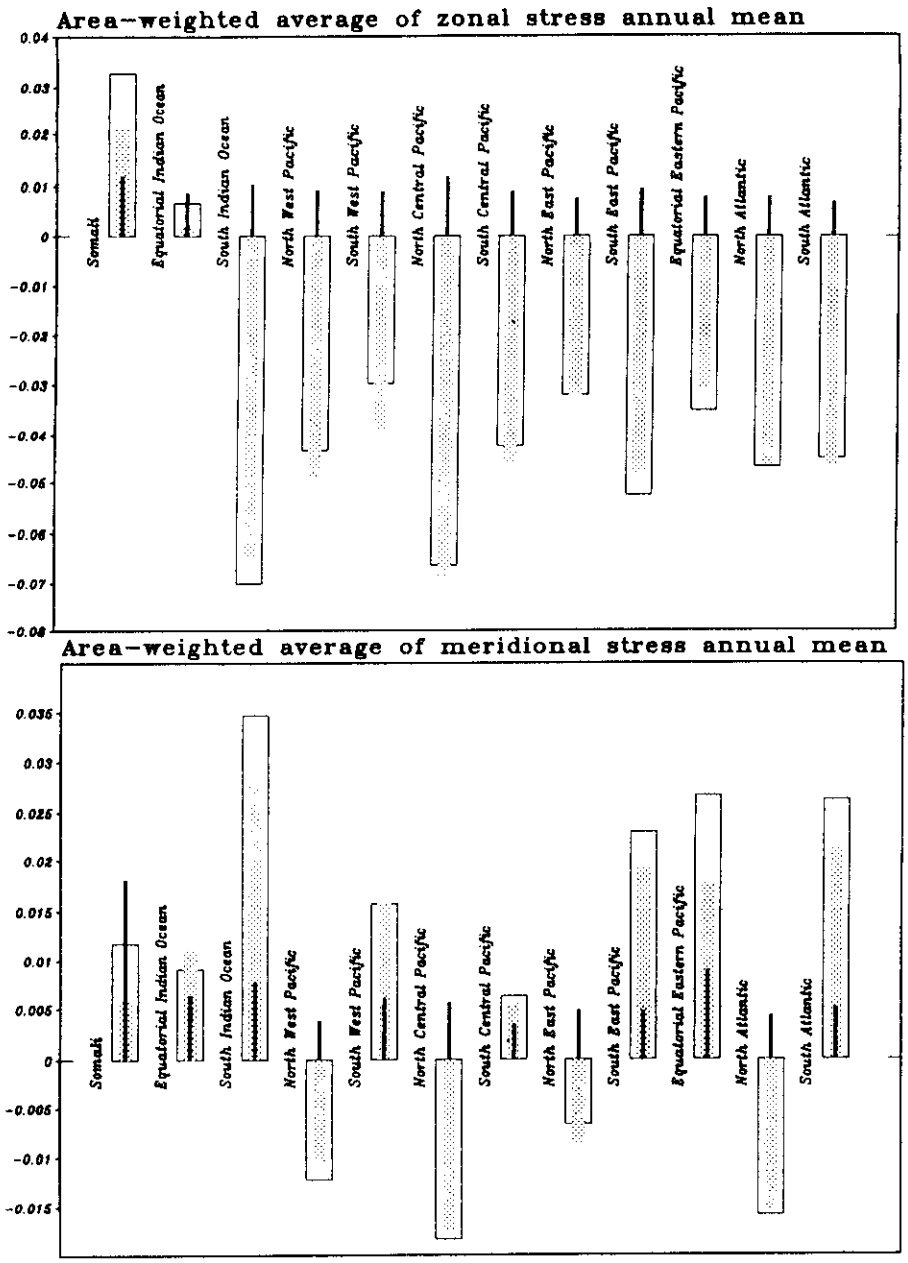

Figure 4: Observed mean (outlined bar), common model mean (grey bar) and intermodel spread (dark line) for the tropical area-averaged annual mean zonal and meridional stresses (Nm^{-2}) at 12 tropical subdomains.

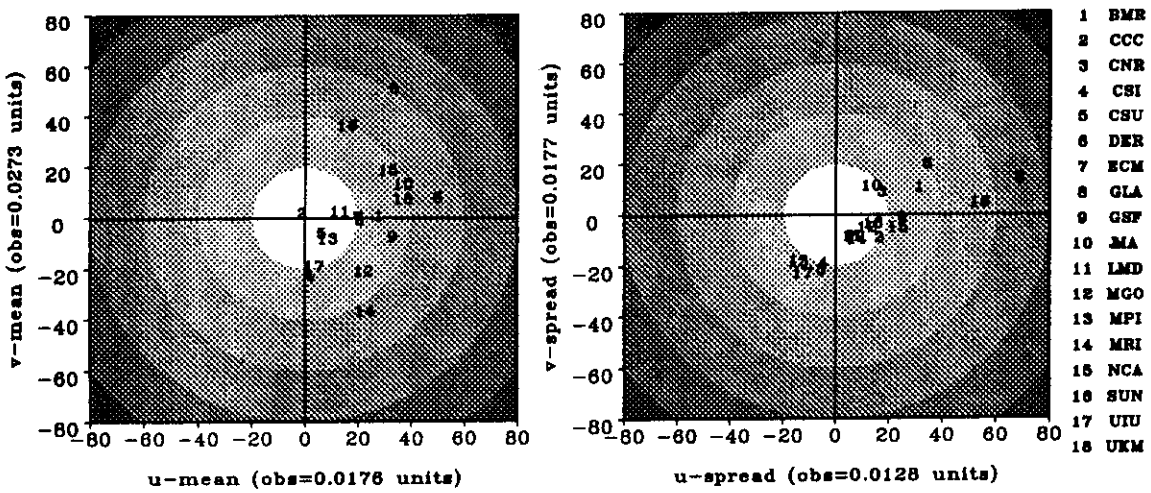

Figure 5: Tropical area-averaged mean and standard deviation (spread) of zonal and meridional stress (Nm^{-2}) annual variance fields for the 18 models plotted as a percentage deviation from the observed value.

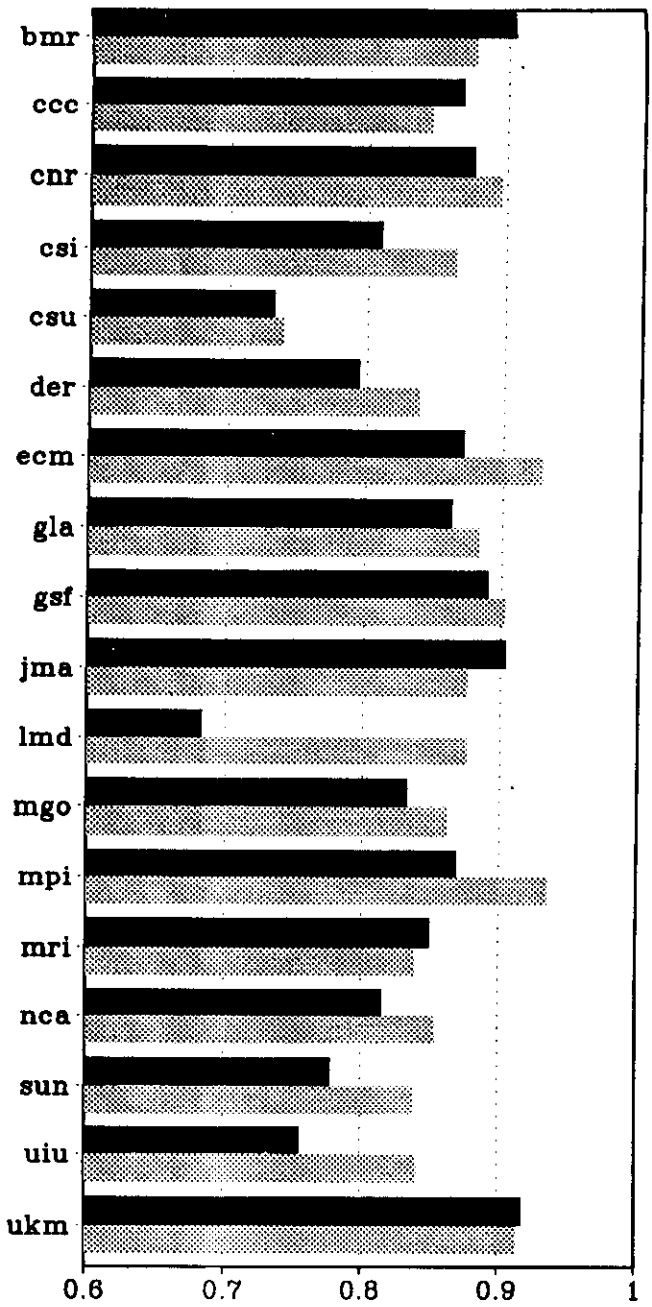

Figure 6: Correlations between model simulated and observed fields of annual variance spatial anomalies. Dark bars measure the correlation coefficient for the zonal component while grey bars measure that for the meridional component.

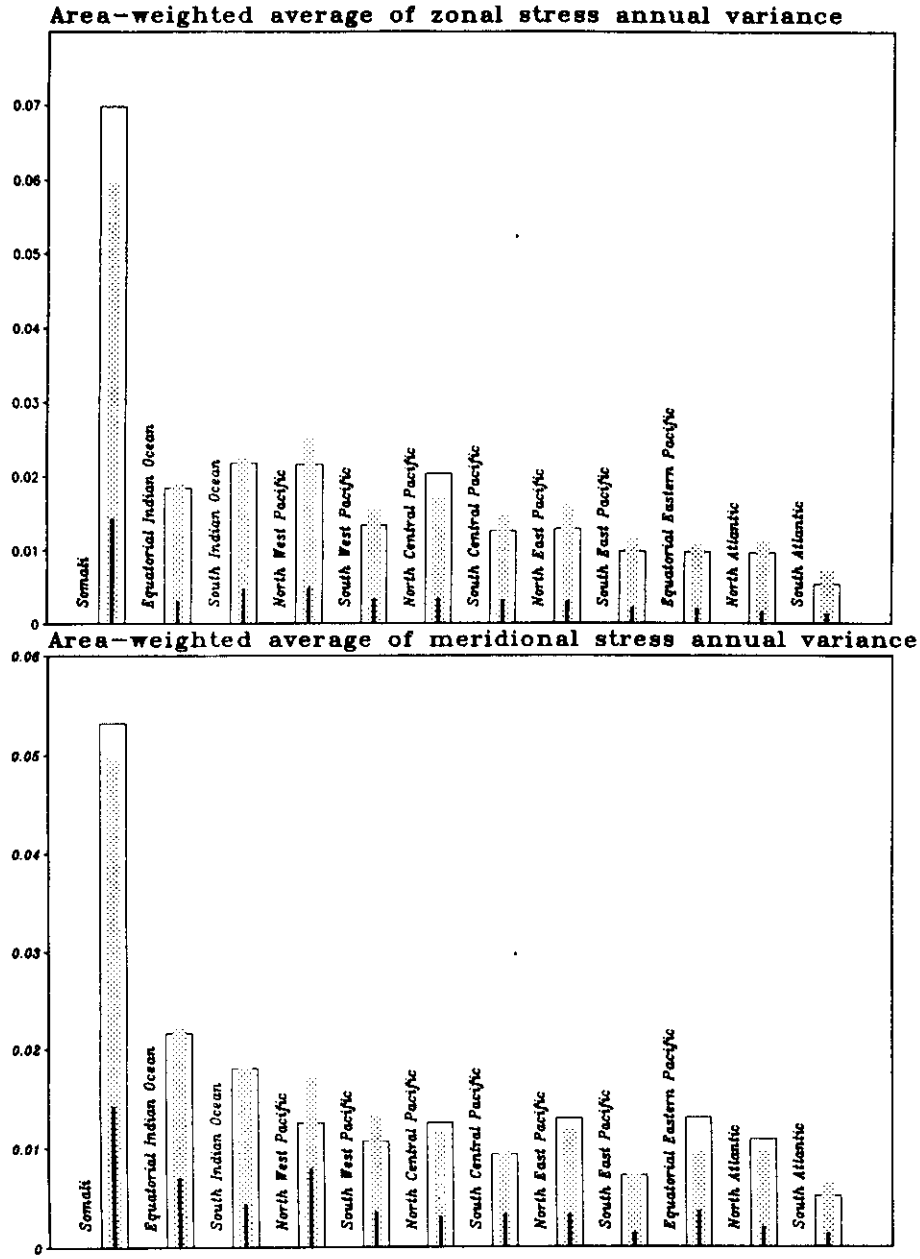

Figure 7: Observed mean (outlined bar), common model mean (grey bar) and intermodel spread (dark line) for the tropical area-averaged zonal and meridional annual variances (Nm^{-2}) at 12 tropical subdomains.

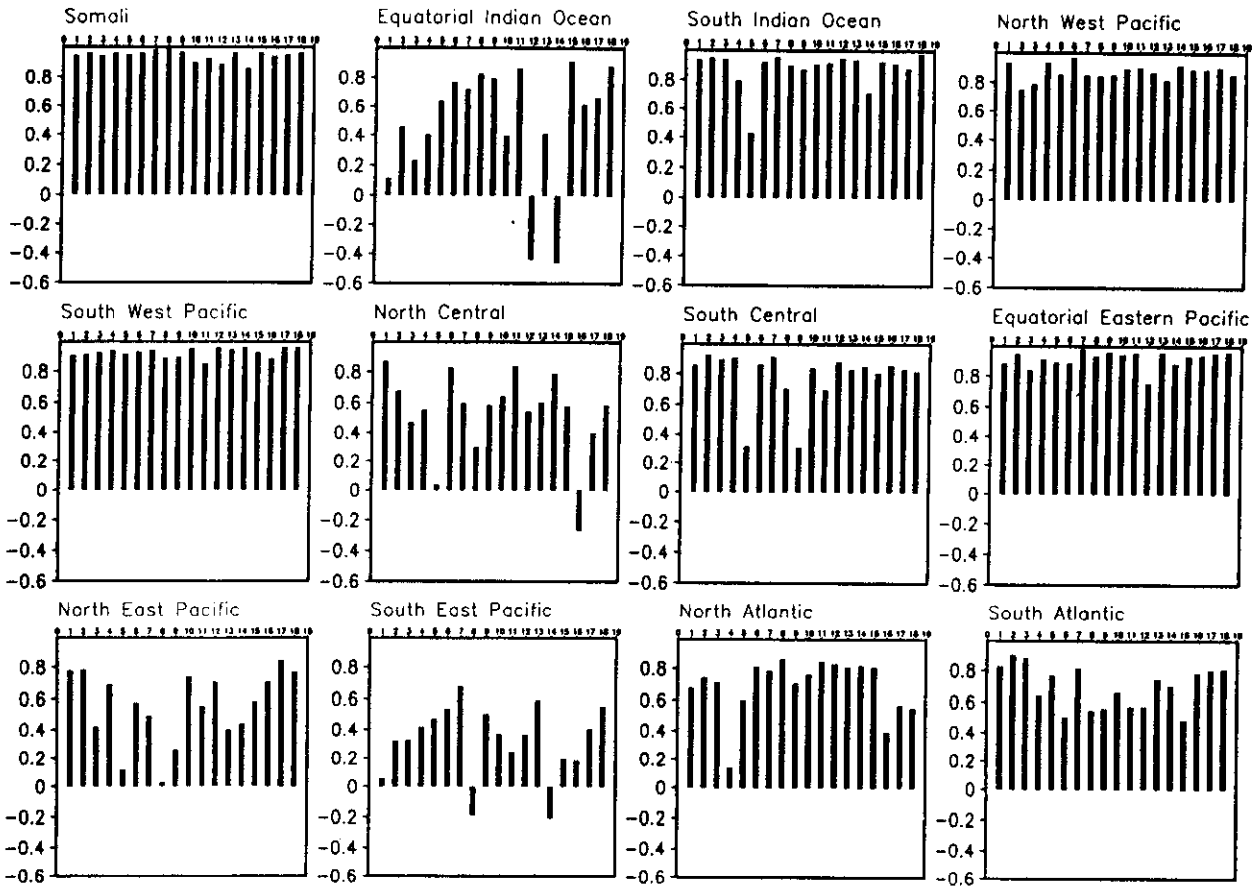

Figure 8: Correlation coefficients between simulated monthly anomalies of zonal wind stress from it's annual mean and observations for the 18 models at the 12 tropical subdomains. The model identification numbers (1 to 18) are same as those shown in fig. 5.

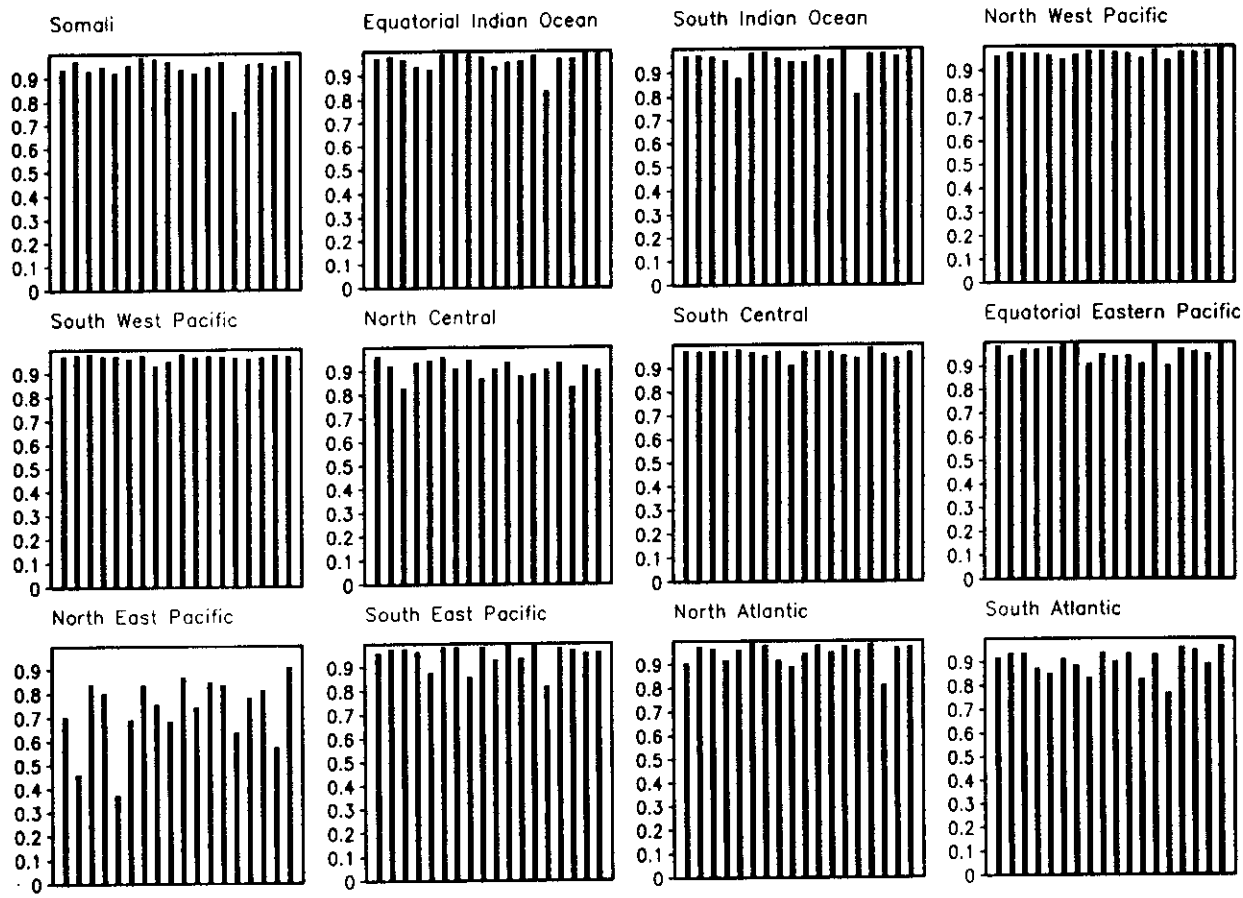

Figure 9: Correlation coefficients between simulated monthly anomalies of meridional wind stress from it's annual mean and observations for the 18 models at the 12 tropical subdomains. Please Model identification number (1 to 18) are same as those shown Fig. 5.

11. Put these numbers!

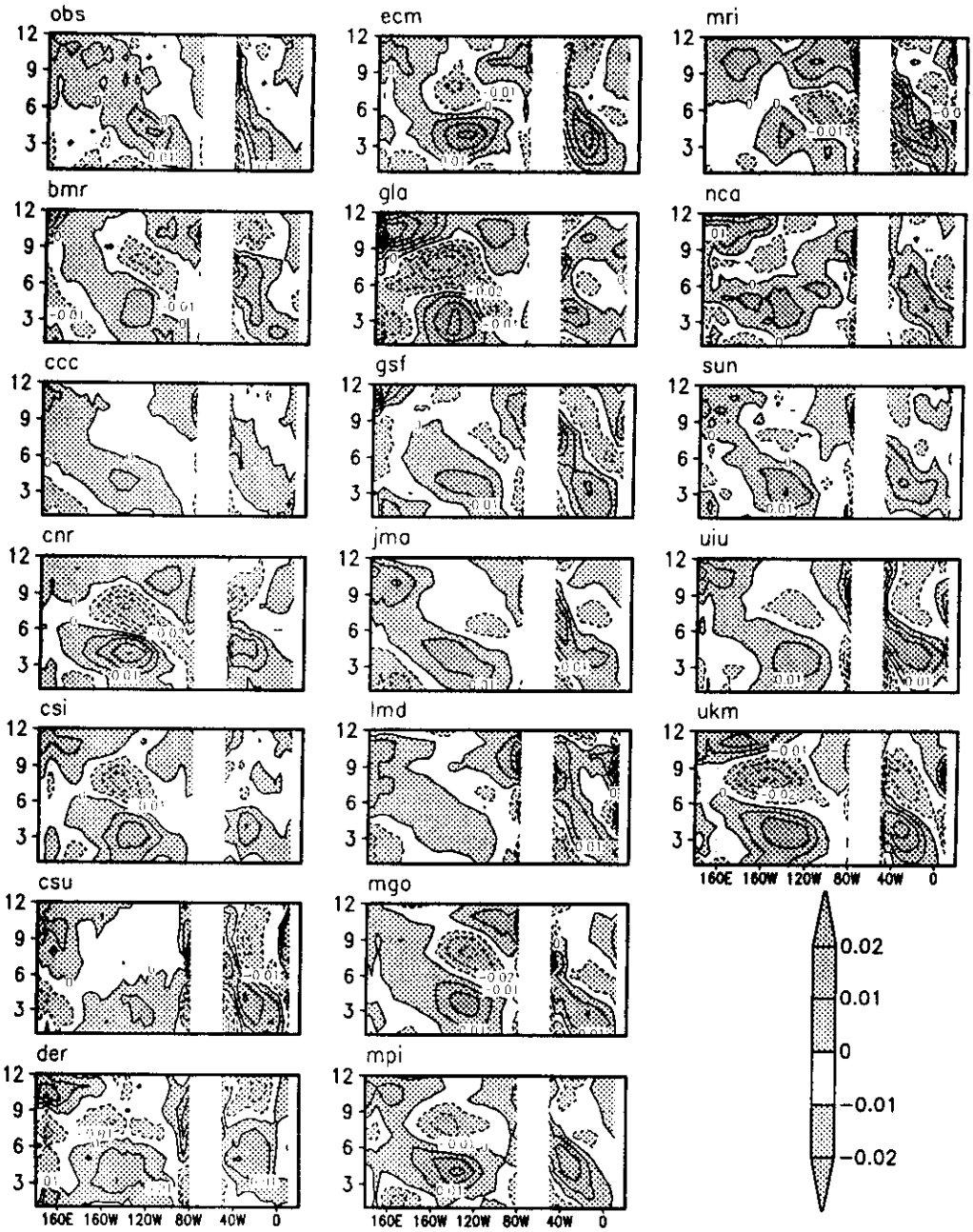

Figure 10: Time-longitude section of zonal stress anomalies (Nm^{-2}) (departure of monthly means from annual mean) averaged between 5°S-5°N in the Pacific and Atlantic basins.

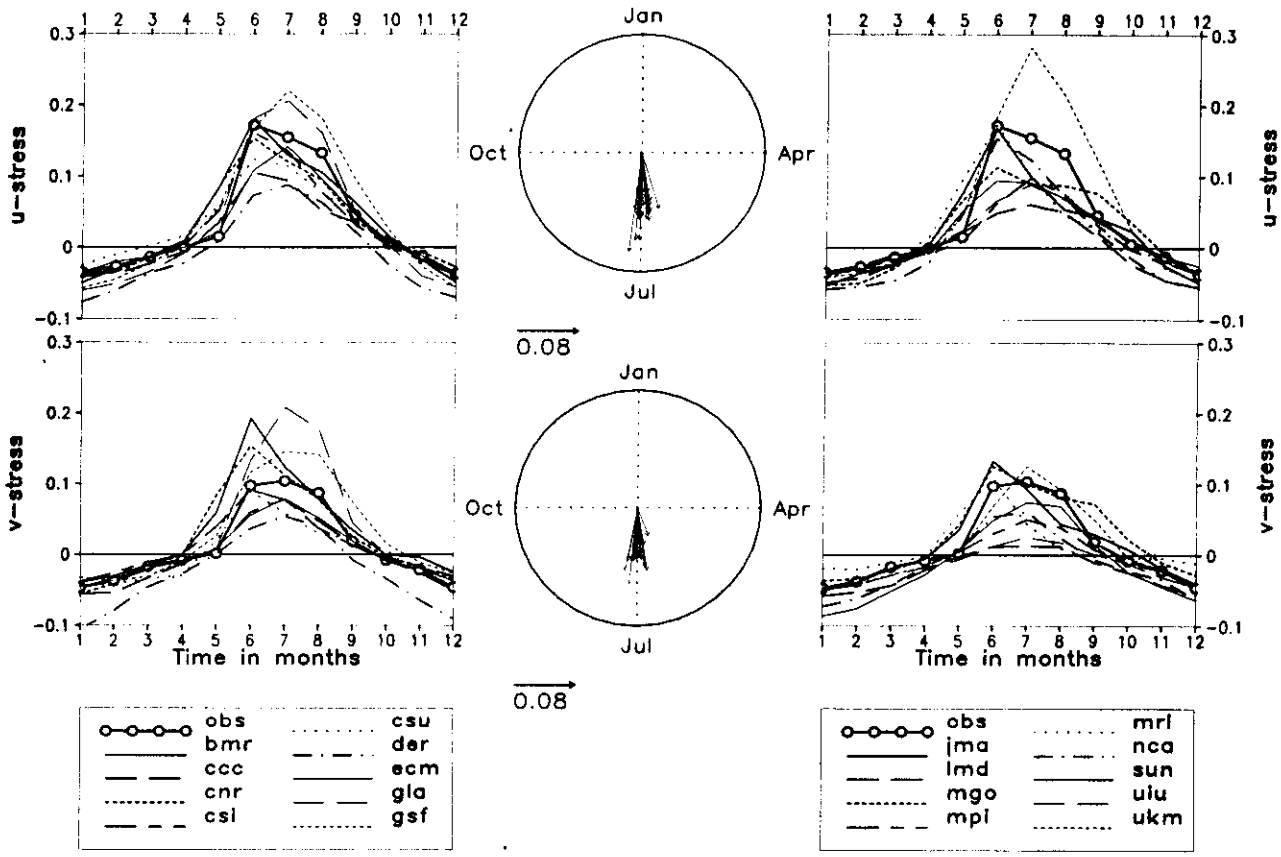

Figure 11: Annual time-series of zonal and meridional monthly mean stresses (Nm^{-2}) averaged over Somali. The corresponding annual harmonics are plotted in the middle, with the thick arrow representing that of the observations and the thin arrows representing that of the different models.

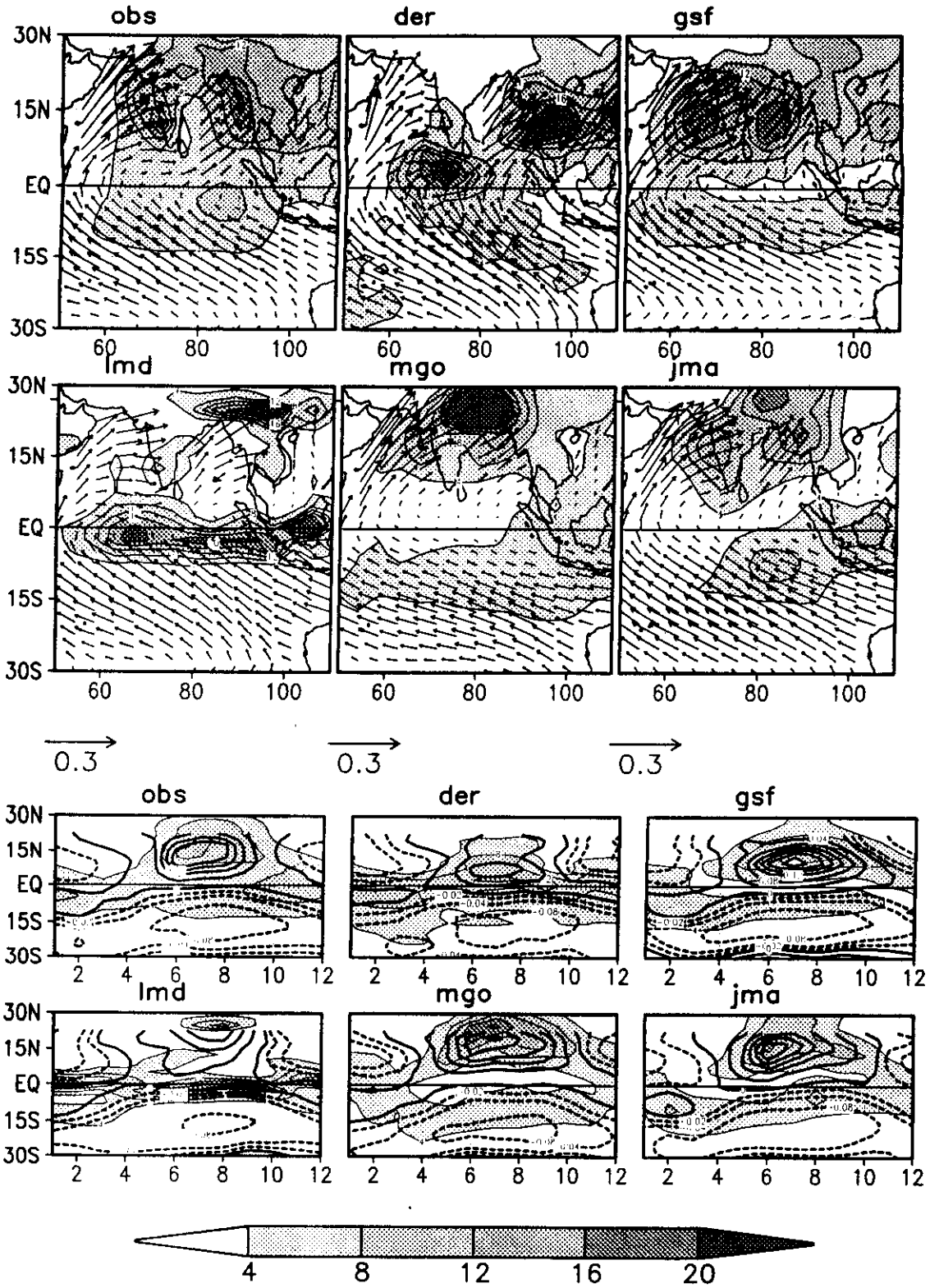

Figure 12: Monthly mean precipitation (shaded contours) and vectors of surface stress (Nm^{-2}) from observations and from 5 selected model simulations for July. The time-latitude section of precipitation (shaded contours) versus zonal stress (in thick contours) is shown in the bottom panel.

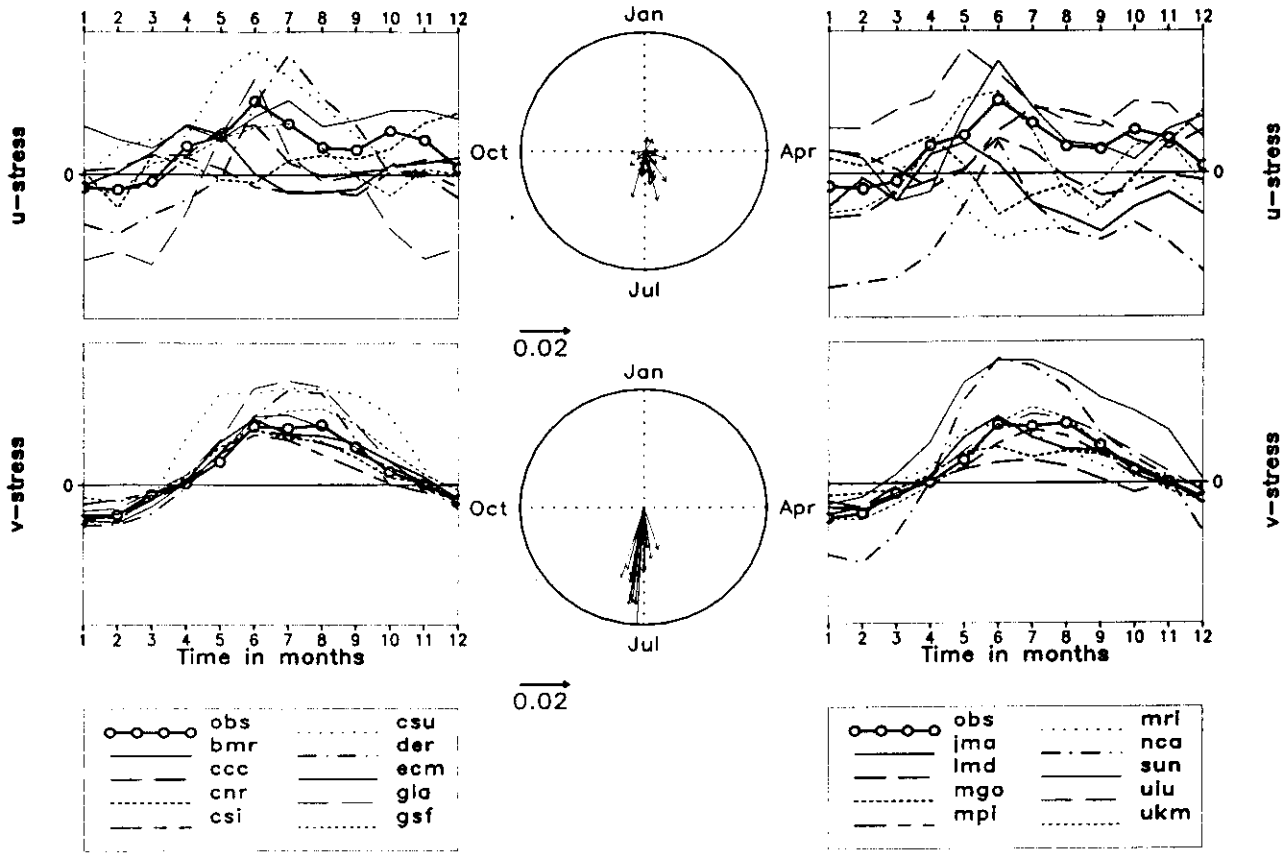

Figure 13: Same as fig 11 but for the equatorial Indian ocean.

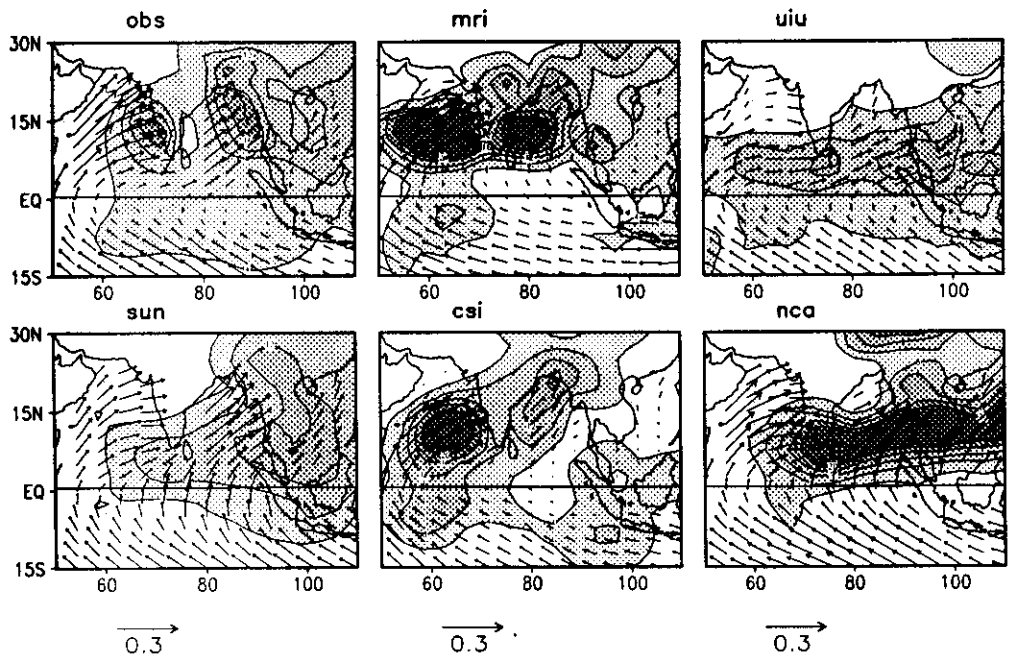

Figure 14: Monthly mean precipitation (shaded contours) and vectors of surface stress (Nm^{-2}) from observations and from 5 selected model simulations for June.

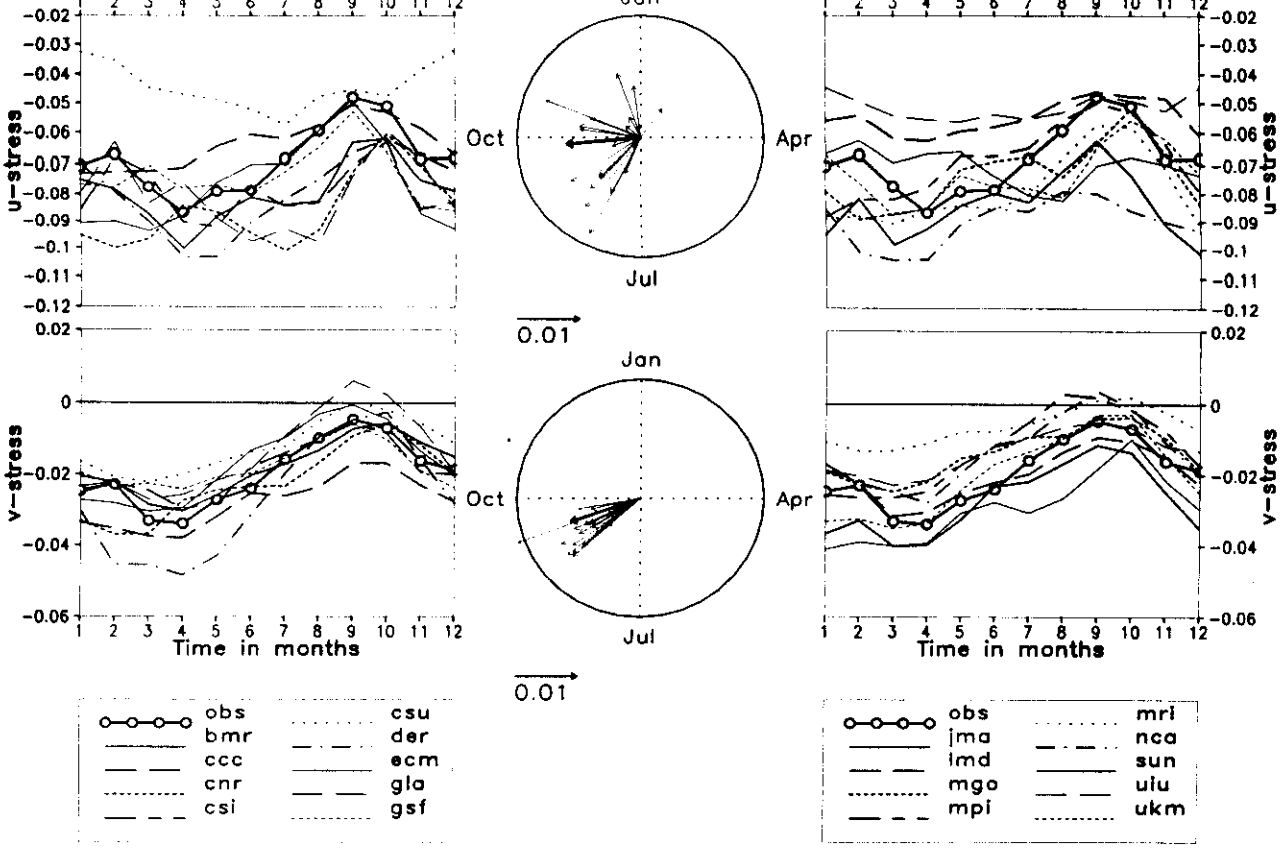

Figure 15: Same as in fig 11 but for the North Central Pacific.

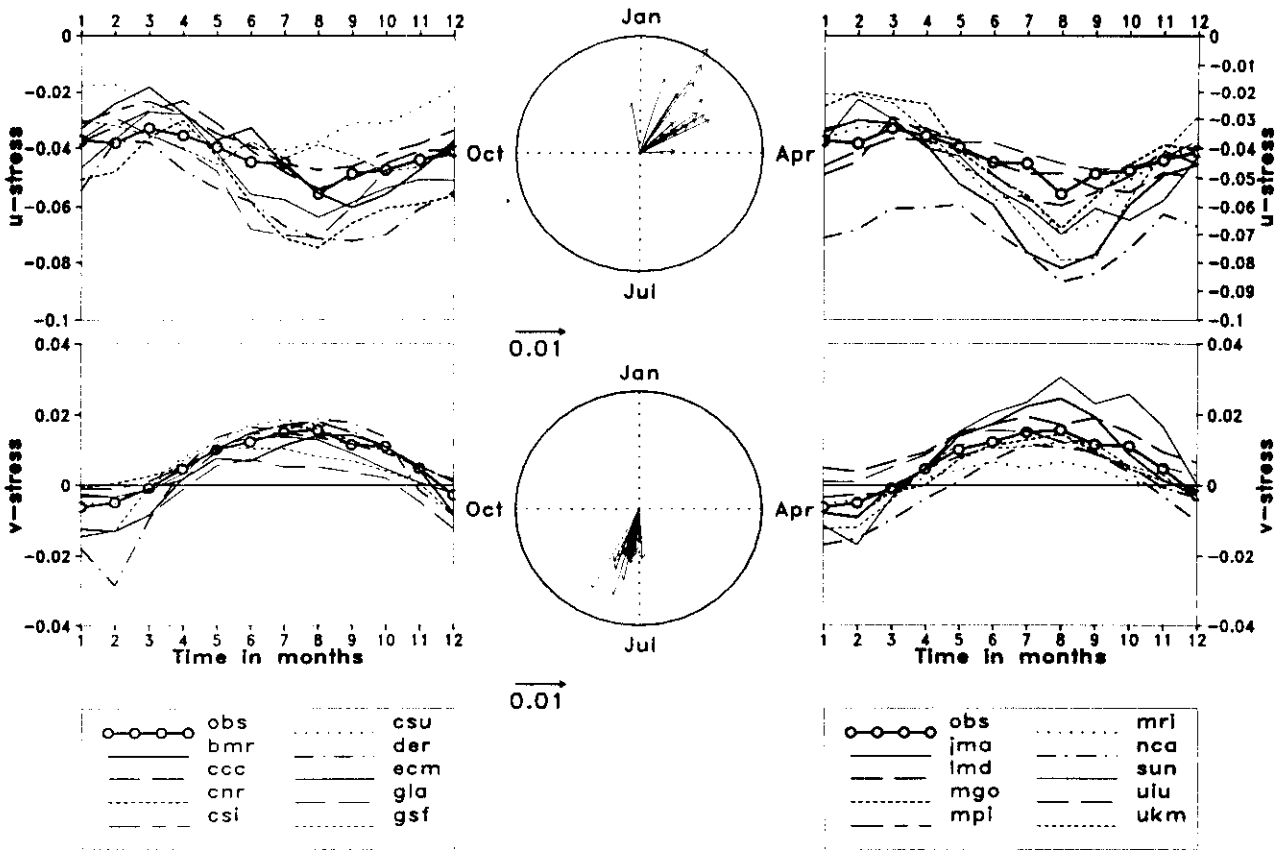

Figure 16: Same as in fig 11 but for the South Central Pacific.

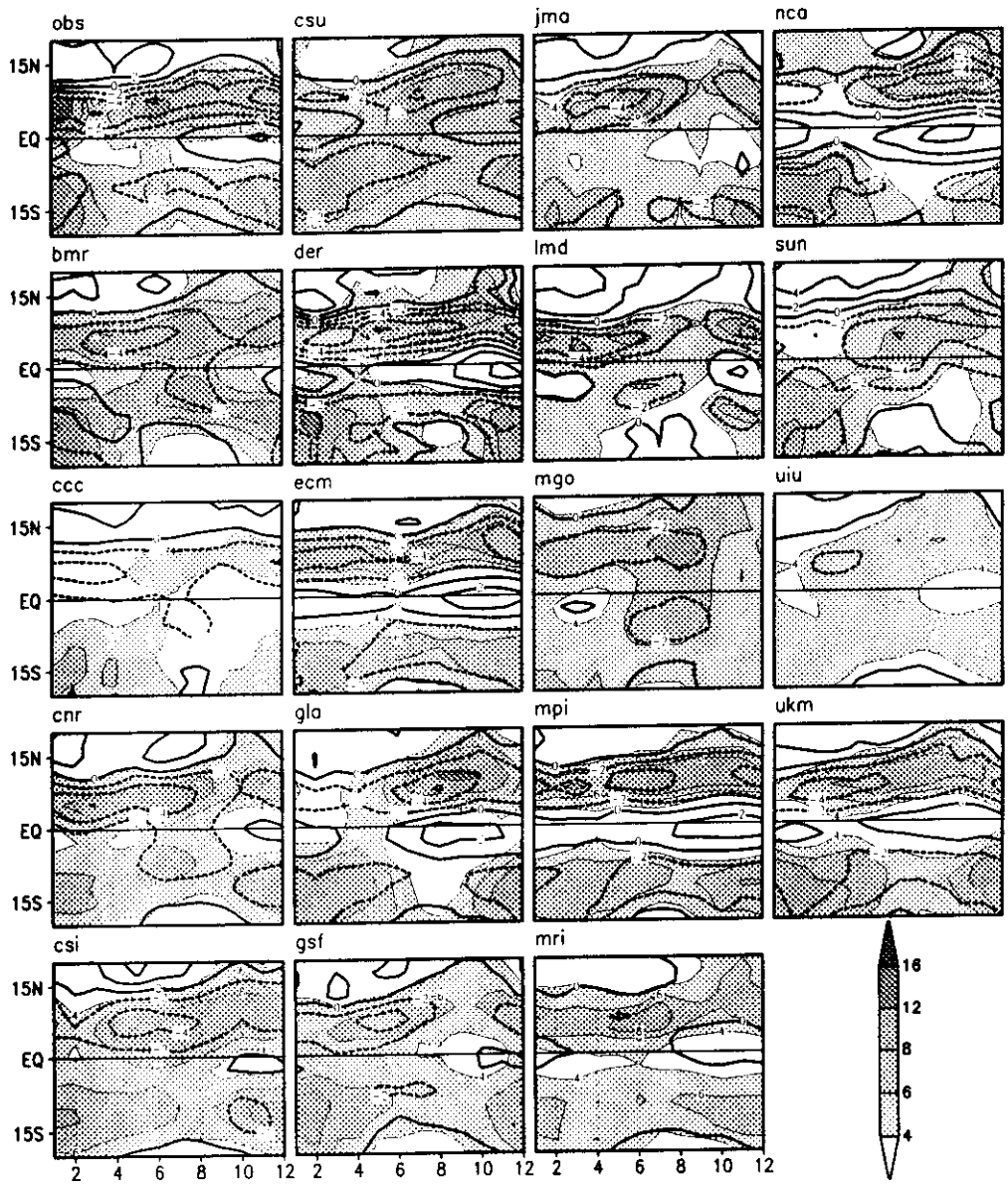

Figure 17: Time-latitude section of longitudinally-averaged (over 180°-140°W) precipitation (shaded thin contours, mm/day) and stress divergence (Nm^{-3}) multiplied by 10^7 (thick contours) in the Central Pacific.

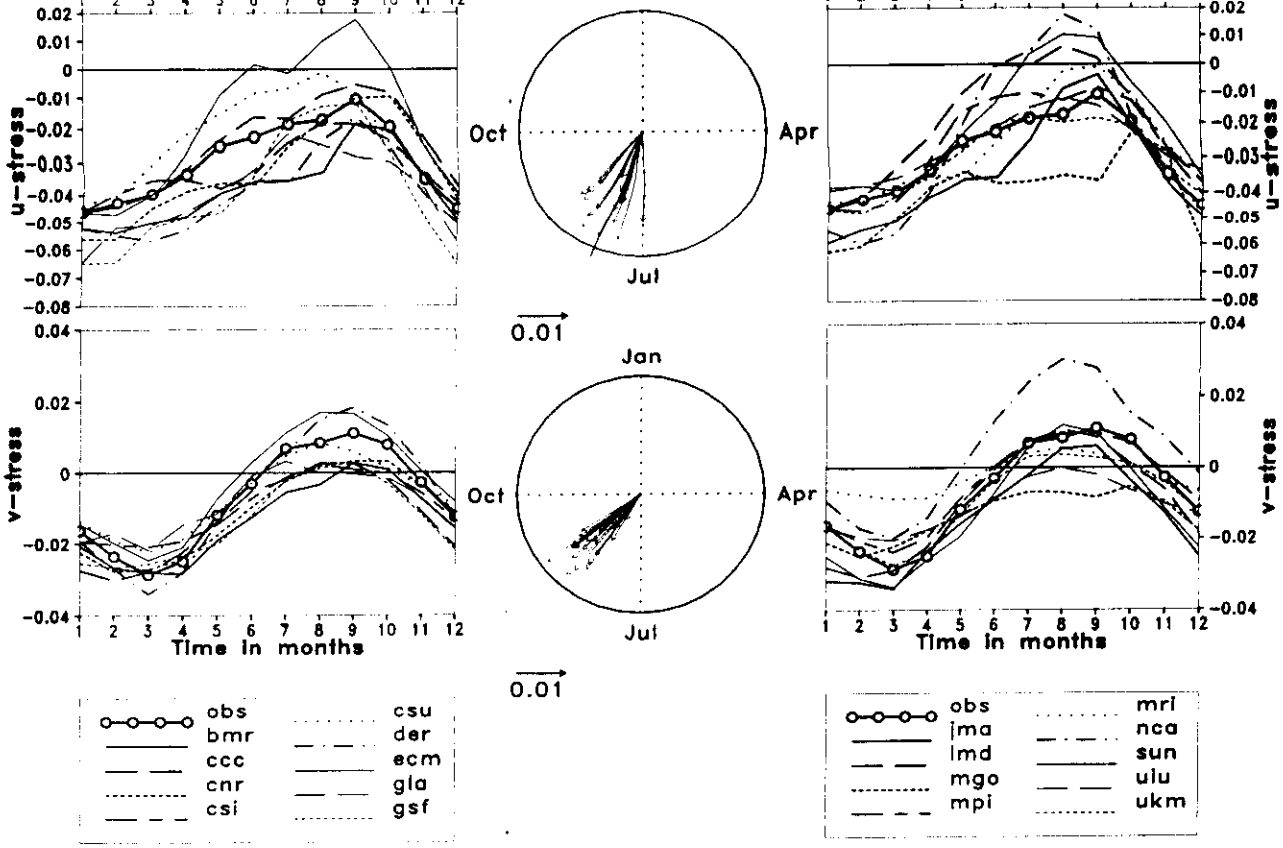

Figure 18: Same as in fig 11 but for the North East Pacific.

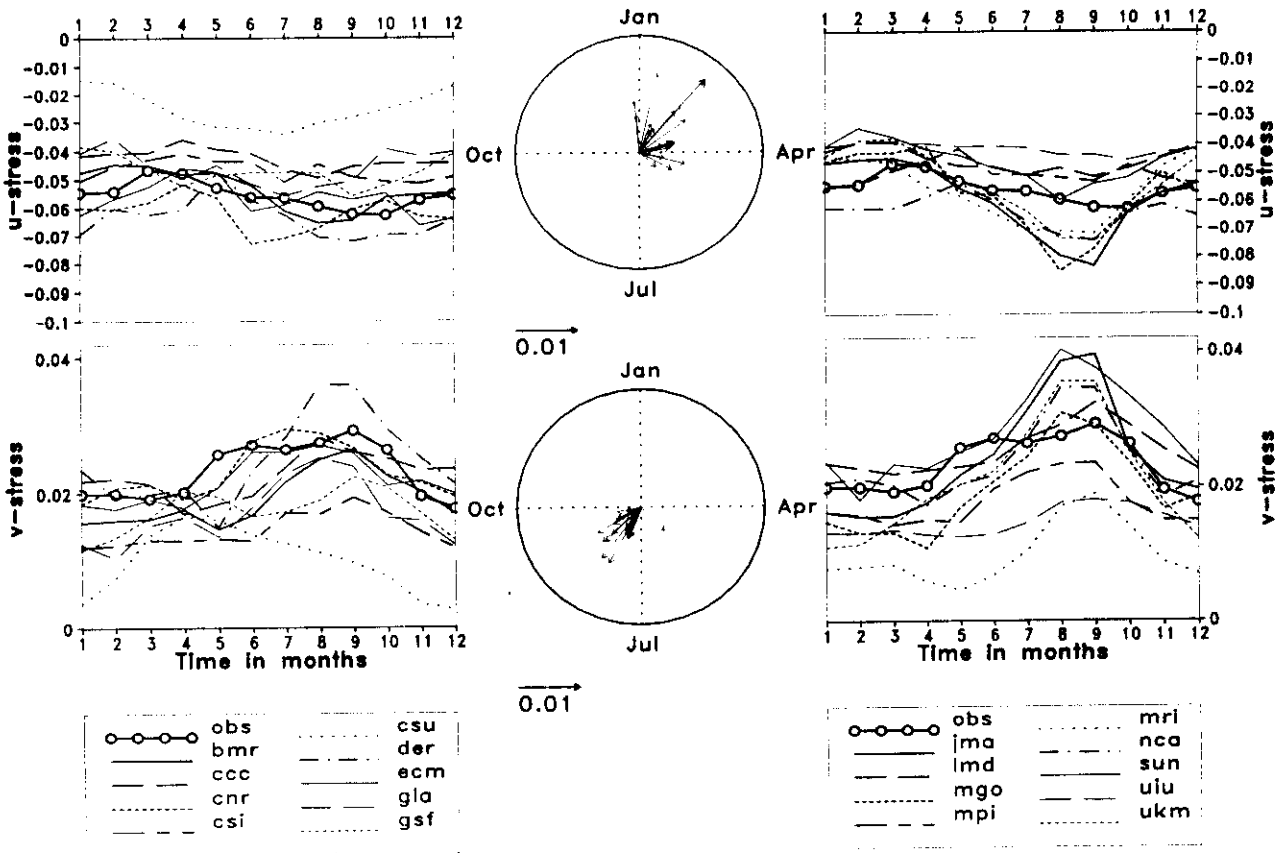

Figure 19: Same as in fig 11 but for the South East Pacific.

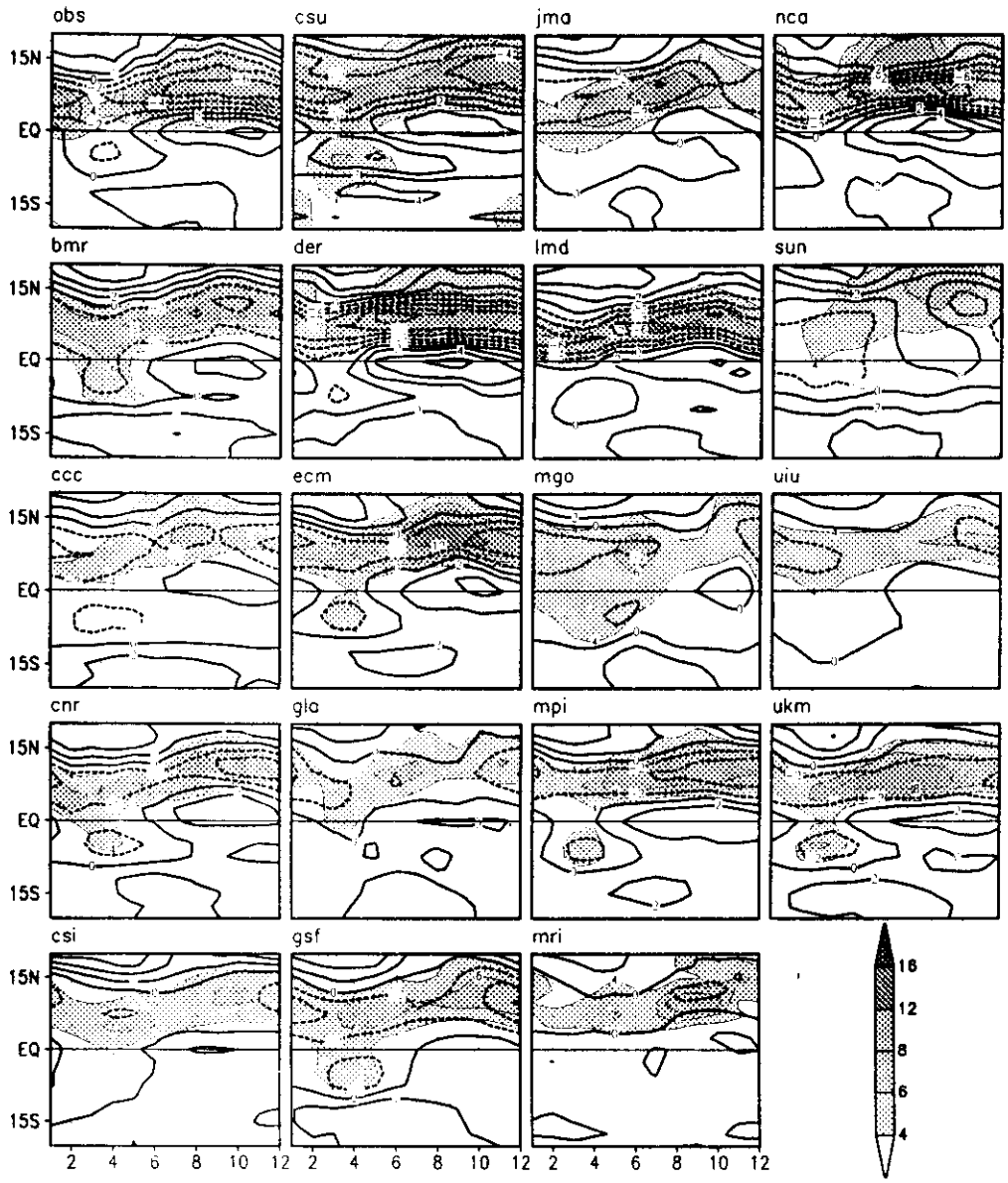

Figure 20: Time-latitude section of longitudinally-averaged (over 140°W-80°W) precipitation (shaded thin contours, mm/day) and stress divergence(Nm^{-3}) multiplied by $10^{o}7$ (thick contours) in the Eastern Pacific.